Supplementary Information for

Stabilization of amyloidogenic immunoglobulin light chains by small molecules

Gareth J Morgan[a,‡,*], Nicholas L Yan[a,‡], David E Mortenson[a], Enrico Rennella[b], Joshua M Blundon[a], Ryan M Gwin[a], Chung-Yon Lin[a], Robyn L Stanfield[c], Steven J Brown[d], Hugh Rosen[d], Timothy P Spicer[e], Virneliz Fernandez-Vega[e], Giampaolo Merlini[f], Lewis E Kay[b,g], Ian A Wilson[c,h], Jeffery W Kelly[a,h,*]

[a]Departments of Molecular Medicine and Chemistry, The Scripps Research Institute, La Jolla, CA 92037
[b]Departments of Molecular Genetics, Biochemistry and Chemistry, The University of Toronto, Toronto, ON, Canada M5S1A8
[c]Department of Integrated Structural and Computational Biology, The Scripps Research Institute, La Jolla, CA 92037
[d]Department of Molecular Medicine, The Scripps Research Institute, La Jolla, CA 92037
[e]Department of Molecular Medicine, The Scripps Research Institute, Jupiter, FL 33458
[f]Departments of Molecular Medicine and Amyloidosis Research and Treatment Center, University of Pavia, and Foundation IRCCS Policlinico San Matteo, Pavia, Italy
[g]The Hospital for Sick Children, Program in Molecular Medicine, 555 University Avenue, Toronto, ON, Canada M5G 1X8
[h]The Skaggs Institute for Chemical Biology, The Scripps Research Institute, La Jolla, CA 92037

‡ identifies co-first authors
* identifies corresponding authors

This PDF file includes:

Supplementary Materials and Methods

Supplementary NMR analysis

Figs. S1 to S20

Tables S1 to S3

References

Other supplementary materials for this manuscript include

Dataset S1

www.pnas.org/cgi/doi/10.1073/pnas.1817567116

SI Materials and Methods

Protein expression and purification

Full-length LCs were expressed as inclusion bodies in *E. coli* as previously described (1). Briefly, inclusion bodies were isolated from cells by five rounds of sonication and centrifugation; dissolved in 4 M GuHCl containing 5 mM DTT; refolded by dropwise dilution into Tris-Cl at pH 8.5 containing 5 mM reduced glutathione and 0.5 mM oxidized glutathione; and purified by ammonium sulfate precipitation followed by ion exchange and size exclusion chromatography. LC V-domains were expressed in the periplasm of *E. coli* using a pelB leader sequence; isolated by periplasmic shock; and purified by ammonium sulfate precipitation followed by ion exchange and size exclusion chromatography.

ALMC2 LC was purified after secretion from the ALMC2 plasma cell line (2). ALMC2 cells were grown in Iscove's modified Dulbecco's media (IMDM) containing 5% fetal bovine serum (FBS), 292 µg/ml glutamine, 100 U/ml penicillin, 100 µg/ml streptomycin and 2 ng/ml nM interleukin-6 (Thermo). Approximately 450,000,000 cells (300 ml of culture) were pelleted and resuspended in 300 ml of IMDM lacking FBS and phenol red indicator, but containing glutamine, penicillin, streptomycin and interleukin-6. Cells were allowed to secrete protein for 24 h, after which cells were removed by centrifugation and filtration. Media containing ALMC2 LC was dialyzed overnight against 25 mM Tris-Cl, pH 8. LC was concentrated by ion exchange chromatography using a FastflowQ column (GE). ALMC IgG was removed by passing the eluate through a protein A column (GE), and the LC was dialyzed and then purified by ion exchange chromatography using a MonoQ column (GE).

5J8 Fab was expressed in HEK293F suspension cells and purified by Ni-NTA and ion exchange chromatography as previously described (3).

Protein labeling

Surface-exposed cysteine residues were incorporated into LCs by mutation using the Novagen QuikChange or NEB SDM mutagenesis protocols according to the manufacturers' instructions. LCs (20-50 μM) were expressed as described above and conjugated with fluorescein by reaction with equimolar fluorescein maleimide (Vector Laboratories) for 1 h at room temperature (22 °C). Unreacted fluorescein was removed by ion exchange chromatography. Labeling efficiency was determined to be 50% by absorbance spectroscopy, corresponding to a single fluorescein molecule per LC dimer. We were unable to improve the labeling efficiency, or fully characterize the conjugated protein by mass spectrometry, which reveals a complex mixture of species. LC misfolding (4) or modification of K83C LCs by glutathione upon refolding may account for some of the heterogeneity. However, our preliminary experiments (Fig. 1) showed that proteolysis of the LCs resulted in a sufficiently large change in fluorescence polarization, so we did not attempt to optimize the labeling and purification further.

Proteolysis assays

Unless otherwise described, LCs were incubated with proteinase K (100 nM; Thermo) in phosphate buffered saline (PBS, 10 mM Na_2HPO_4, 1.8 mM KH_2PO_4, 137 mM NaCl, and 2.7 mM KCl, pH 7.4), after which the reaction was quenched with phenylmethyl sulfonyl fluoride (100 μM) and remaining LC quantified by SDS-PAGE or fluorescence polarization. The experiment in Fig. 1b measured simultaneous proteolysis of labeled and unlabeled LC by adding 20 nM WIL-FL* or JTO-FL* to 5 μM WIL-FL or JTO-FL, respectively. Fluorescein fluorescence images of the SDS-PAGE gels were recorded, after which the gels were Coomassie stained and imaged. Gel images shown have had their contrast increased after quantification for clarity.

Fluorescence polarization measurements

FP in cuvettes was measured in a Jasco 8600 fluorimeter fitted with polarizing filters and excitation and emission monochromators, using an excitation wavelength of 488 nm and emission wavelength of 520 nm. FP on plates was measured using a Perkin Elmer EnVision plate reader equipped with polarizing excitation and emission filters (λ_{ex} = 485±20 nm, λ_{em} = 535±20 nm) and a 505 nm dichroic mirror. Fluorescein-labeled LC (20 nM) in PBS containing 0.02% (v/v) Pluronic F-127 detergent (Thermo) was used for all measurements. Fluorescence polarization was calculated using the formula:

1) $P = G\frac{FS-FP}{FS+FP}$

Where P is the polarization, FS and FP are the emission intensities of parallel and perpendicular-polarized light, respectively, and G is a dye- and instrument-specific correction factor. Total fluorescence was calculated using the formula:

2) $TF = FS + 2FP$

Addition of detergent appears to prevent denaturation of the LC upon binding to the polystyrene surface of the plate, since it did not affect the kinetics of proteolysis in quartz cuvettes (SI Appendix Fig. S2).

Pilot screen

For screening in a plate format, each compound's effect on the PK proteolysis of WIL-FL* was measured by FP after 24 h incubation at room temperature (typically 22 °C). The measured FP was normalized platewise by comparing the compound wells to high and low control wells on each plate (n=32). The high FP control wells contained JTO-FL* and DMSO vehicle without proteinase K. Low FP control wells contained WIL-FL*, DMSO vehicle and proteinase K, to determine the rate of proteolysis of unliganded WIL-FL*. Percent activity was calculated for each plate using the formula:

3) $Percent\ activity = 100 \times \frac{Test\ well - median(data\ wells)}{Median(high\ control) - median(data\ wells)}$

To screen the Maybridge Hitfinder library, WIL-FL* and JTO-FL* in PBS, pH 7.4, containing 0.02% Pluronic F-127 detergent were dispensed into black polystyrene microplates (Greiner catalog # 788076) using a Beckman Coulter BioRAPTR. Final LC concentration was 20 nM in 10 µl, equivalent to 10 nM fluorescein. Compounds (n=1) were added by 50 nl pintool from 10 mM DMSO stock solutions using a Beckman Coulter BioMek robot for a final concentration of 10 µM compound and 0.5% DMSO. Plates were incubated at room temperature (22 °C) for 10 min to allow compounds to dissolve, after which proteinase K was dispensed to a final concentration of 500 nM. Plates were centrifuged at 1000 rpm for 1 minute, stacked, wrapped to minimize evaporation, and incubated for 24 h at 22 °C. FP was measured as described above. We used hits from the Maybridge screen (compounds **17** and **18**, SI Appendix Table S1) to validate the assay for use on 1,536-well plates.

Primary screen

653,085 small molecules from the Scripps Florida screening library were screened using the PCFP assay in 1,536-well plates. Final LC concentration was 10 nM in 5 µl. Small molecules were added by pintool from DMSO stock plates to a final concentration of 6.75 µM compound and 0.675% DMSO. Activity relative to the high control (JTO-FL* with no protease) and low control (WIL-FL* with DMSO vehicle) was calculated using equation 3, above. 2,779 small molecules were selected as hits based on an activity greater than three standard deviations above the mean activity of the plate. This result corresponds to an initial hit rate of 0.4%. Assay performance was consistent with a platewise average Z' of 0.75 ± 0.03 and an average signal-to-background ratio of 1.36 ± 0.02 (mean ± sd, n=526 plates). Two compounds were unavailable for further study, so 2,777 small molecules were replated at 10 mM in DMSO to create a stock plate for secondary screens.

Secondary screens

We used three rounds of secondary screening to remove false positive hits from the primary screen. The 2,777 small molecules identified in the primary screen were used for each secondary screen.

Firstly, the PCFP assay was repeated in triplicate with each of the 2,777 primary screening hits, with an average Z' of 0.71 ± 0.03. We identified 1,422 molecules with >20.6% activity (the mean plus three standard deviations of this dataset). Note that many compounds show apparent protection greater than the JTO-FL* positive control, which we attribute to autofluorescence of the small molecule affecting the FP measurement.

Secondly, to remove compounds that interfere with the FP measurement, the primary screen was repeated in triplicate but compounds were added after 24 h of proteinase K treatment (Fig. 1f). This assay had an average Z' of 0.73 ± 0.01. Bona fide hits should retain no FP beyond the low control. Six hundred sixty two small molecules that showed 1.25-fold lower mean activity in this assay compared to the secondary screen described in the previous paragraph were retained.

Thirdly, to remove molecules that inhibit proteinase K, the assay was repeated in triplicate using 100 nM thermolysin (Thermo). The assay was carried out in 50 mM Tris-Cl, pH 7.5, containing 150 mM NaCl, 100 µM $ZnCl_2$, 100 µM $CaCl_2$ and 0.02% v/v Pluronic F-127 detergent. The additional metal ions were added to bind to ion-chelating small molecules and prevent them from inhibiting the metalloproteinase. This assay yielded an average Z' of 0.64 ± 0.02. We identified 1,578 compounds that were active in this assay, which we define as >20 % activity (mean plus three standard deviations of this dataset). Of these, 1,243 molecules showed similar activity against PK and thermolysin.

Two hundred sixty nine molecules that passed all three secondary screens were retained for further analysis. We also retained 147 additional molecules that passed the FP artefact secondary screen but

failed one of the two other secondary screens assessing protease inhibition (PCFP with PK or with thermolysin). Data for all 416 samples are shown in Supplementary Dataset 1.

The concentration-dependence assay employed the same reagents, protocols, and detection systems as the secondary assays, but tested each of the selected compounds as 10-point dose-response titrations (3-fold dilutions) in triplicate, in each of the three formats described above. A four-parameter equation describing a sigmoidal dose-response curve was then fitted with adjustable baseline using Assay Explorer software (Symyx Technologies Inc.). The reported EC_{50} values were generated from fitted curves by solving for the X-intercept value at the 50% activation level of the Y-intercept value. Small molecules which showed similar concentration dependent FP retention in the PK and thermolysin screens and contrasting activity in the FP artefact counterscreen were retained.

All compounds used for titration assays were analyzed by LC-MS to confirm purity and identify mass. Of the 416 samples submitted for LC-MS analysis, 386 samples confirmed mass, i.e., the molecular weight of the structure in Scripps' database matched that identified by LC-MS analysis of the screening sample. As determined by nominal methods (UV-vis spectroscopy, MS and ELSD), 379 samples demonstrated purity of >80%.

Protease inhibition assay

PK (5 µl of 200 nM), or buffer without protease, were dispensed into wells of a microplate. Compounds were added by pintool (n=2) and incubated for 5 min at room temperature (22 °C). Five µl of EnzCheck Red fluorogenic protease substrate (Thermo) were dispensed into the wells. Fluorescence (λex = 580 nm, λem = 620 nm) was read at 30 sec intervals for 5 min. An increase in fluorescence indicated protease activity. Endpoint fluorescence is reported in SI Appendix Fig. S3. Some compounds exhibit an apparently higher protease activity than vehicle, which we attribute to autofluorescence.

Equilibrium dialysis

Eight compounds were dialyzed against 20 µM WIL-FL in PBS containing 0.02% Pluronic F-127 detergent in 8 kDa-cutoff Rapid Equilibrium Dialysis cartridges (Thermo) for 4 h according to the manufacturers' instructions. Small molecule concentrations inside and outside the dialysis cartridge were measured by reverse phase HPLC and dissociation constants calculated using the equation:

4) $$K_D = \frac{[LC] \times [Ligand_{out}]}{[Ligand_{in}] - [Ligand_{out}]}$$

Where [LC] is the LC concentration inside the dialysis cartridge, [$Ligand_{in}$] and [$Ligand_{out}$] are the measured small molecule concentrations inside and outside the dialysis cartridge, respectively.

Isothermal Titration Calorimetry (ITC)

WIL-FL was dialyzed into PBS, and the dialysate was filtered and used to dilute the LC and small molecules for ITC analysis. DMSO and Pluronic F-127 concentrations were matched as closely as possible between the protein and ligand solutions. Small molecule (100 µM) was titrated into 20 µM LC (monomer equivalent) with a Microcal Auto ITC 200. Heats were analyzed using Origin software (OriginLab Corporation).

Fluorogenic coumarin titration

LCs were concentrated to 200 µM in centrifugal concentrators with a 10 kDa membrane, unless the available material was limiting. 1.5-fold serial dilutions of LCs in PBS containing 1 µM **1** and 0.02% (v/v) Pluronic F-127 were prepared in 384-well plates. Fluorescence of **1** was measured on a Gemini plate reader (Molecular Devices) using an excitation wavelength of 373 nm and emission wavelength of 445 nm. Data were normalized platewise to the plateau fluorescence value for WIL-FL to calculate the fraction of **1** bound. These data were initially fit to a 2-state, 1-site binding equation:

5) $$fraction\ bound = \frac{[LC]}{K_{D\ ligand} \times [LC]}$$

where $K_{D\ ligand}$ is the LC•**1** dissociation constant. For LCs lacking an inter-chain disulfide bond, **1** binds to the dimer and shifts the monomer-dimer equilibrium towards dimer (Fig. 2e and SI Appendix Fig. S6). To estimate the affinity of the e fit the fluorescence data to a 3-state, 1-site binding equation:

6) $$fraction\ bound = \frac{[LC]^2/K_{D\ dimerization}}{K_{D\ ligand} \times [LC]^2/K_{D\ dimerization}}$$

where the dimerization dissociation constant, $K_{D\ ligand}$, is constrained to 1-10 μM based on NMR affinity measurements (5).

Analytical Ultracentrifugation (AUC)

WIL-FL and WIL-V (20 μM) in PBS containing either 0.5% DMSO vehicle or 100 μM **1** were run in a Beckman XL-1 analytical ultracentrifuge at 50,000 rpm at 20 °C. Sedimentation was measured by absorbance at 280 nm. Data were processed using SedFit (6).

Crystal structure determination

Purified JTO-FL was concentrated to 200 μM and subjected to crystallization trials using the high-throughput robotic Rigaku CrystalMation platform at The Scripps Research Institute. Crystals of JTO-FL were grown via sitting-drop vapor diffusion using a crystallization buffer consisting of 20% PEG 3350 and 0.2 M $NH_4H_2PO_4$ at 23 °C. Both diamond-shaped and plate-shaped crystals were generated in the same drop using these conditions, but only the plate-shaped crystals produced usable diffraction data. To generate JTO-FL•**1** complexes, crystals of *apo* JTO-FL were soaked with a tenfold molar excess of **1** for 10 days. Crystals were harvested and immediately flash cooled in liquid nitrogen.

Diffraction data were collected from crystals at 80 K and a wavelength of 1.0332 Å at beamline 23-ID-D (for *apo* JTO-FL) or 23-ID-B (for JTO-FL•**1**) at the Advanced Photon Source (Argonne, IL). Frames were indexed and integrated using HKL-2000 (7) (for *apo* JTO-FL) or XDS (8) (for JTO-FL•**1**), the space group

was assigned as $P2_12_12_1$ using Pointless, and data were scaled in Scala (9). Five percent of reflections (randomly distributed) were flagged for model cross-validation using R_{free} (10).

The *apo* JTO-FL structure was solved to 1.75 Å resolution by molecular replacement (MR) with Phaser (11), using the existing full-length CLE light chain structure (12) (PDB: 1LIL) as the search model. The JTO-FL•**1** structure was similarly solved to 1.8 Å resolution with MR using *apo* JTO-FL as the search model. Both models were refined with iterative cycles of manual adjustment in Coot (13), and refinement in Refmac5 (14) using isotropic thermal parameters and hydrogen atoms at calculated positions. Final adjustments were made after analysis with MolProbity (15). The refined models were deposited in the Protein Data Bank under accession codes 6MG4 for *apo* JTO-FL and 6MG5 for JTO-FL•**1**.

NMR

A stock solution of **1** (40 mM) was made by dissolving the ligand into ethanol. All samples were buffered in 50 mM Bis Tris, pH 6.4, 1 mM EDTA, 10% D_2O. All in-phase (for ^{15}N WIL-V and ^{15}N JTO-V) and TROSY (for ^{15}N WIL-FL) based ^{1}H,^{15}N experiments were recorded at 37 °C on a 14.1 T Bruker AVANCE III HD spectrometer equipped with a cryogenically cooled x,y,z gradient probe.

For the titrations, samples with different protein:**1** ratios were generated starting from two mother solutions, the first without the ligand, the second with a ratio of 1:2.2 between concentration of monomeric protein and ligand. The concentration of ethanol was identical in the two mother solutions. The concentration of monomeric protein was 0.05, 0.4 and 0.14 mM respectively for WIL-FL, WIL-V and JTO-V. Intensities for 8 **LC_2** peaks (Asn 30, Tyr 32, Trp 35, Gln 38, Gly 41, Phe 50, Gly 101) and 4 **LC_2•L** peaks (Asn 30, Gln 38, Gly 41, Asp 52) were fitted to get an estimate of the K_D for WIL-FL.

^{15}N transverse relaxation rates were calculated from R_1 and $R_{1\rho}$ experiments acquired for JTO-V and WIL-V at 0.4 mM protein concentration with or without 1 mM **1**. A ^{15}N γB_1 field of 1.7 kHz was applied during the relaxation delay for $R_{1\rho}$ experiments.

Chemical exchange saturation transfer (CEST) experiments were acquired on WIL-V samples at 0.4 mM in the presence of 0.2 or 0.3 mM **1** using a multi-site excitation scheme (16). 4.25 µs DANTE pulses with γB_1 = 6.4 kHz were applied every 9.1 ms during a saturation delay of 0.35 s, giving an effective ^{15}N B_1 field of 3 Hz and a spacing on 110 Hz between consecutive excitation frequencies. Longitudinal two-spin order ZZ-exchange experiments were acquired on JTO-V samples at 0.14 mM in the presence of 0.06 mM **1**, with the 1-50 ms ZZ-mixing delay occurring after t_1 evolution (17). Further details of the analysis of these experiments are given in the Supplemental NMR Analysis described below.

Native-state hydrogen exchange experiments were measured for WIL-V at 0.2 mM and JTO-V at 0.1 mM with or without 0.5 mM **1**. The proteins, previously desalted and lyophilized, were dissolved in a D_2O based sodium citrate buffer, pD 5.0, containing 1.25% v/v of either pure ethanol or 40 mM **1** stock solution. Per-residue exchange rates k_{ex} were converted to free energies using the equation:

$$7) \quad \Delta G = -RT \ln\left(\frac{k_{ex}}{k_{rc}}\right)$$

where k_{rc} are the residue-specific exchange rates of unprotected amides (18).

Kinetic unfolding

WIL-FL (5 µM) in 50 mM sodium phosphate buffer, pH 7.0, containing 50 µM **5** was rapidly diluted into urea in 50 mM sodium phosphate buffer and 50 µM **5** using an APP SX-20 stopped flow fluorimeter at 37 °C. The change in fluorescence emission >335 nm was measured as a function of time (λ_{ex} = 280 nm). Measurement of unfolding rates in the presence of **1** was not possible on this filter-based fluorimeter due to fluorescence of **1**. Kinetic transients were fitted to single exponential curves and rates extracted.

Equilibrium unfolding

WIL-FL (5 µM) was titrated against urea in 50 mM sodium phosphate buffer, pH 7.0, containing 50 µM **5** or 100 µM **1**. After incubation overnight at 25 °C, intrinsic tryptophan fluorescence emission spectra

were measured using a Jasco 8600 fluorimeter (λ_{ex} = 280 nm, λ_{em} = 300-420 nm). Average wavelength (also known as center of spectral mass) values were calculated using the equation:

8) $$Average\ wavelength\ = \frac{\sum_i \lambda_i \times I_i}{\sum_i I_i}$$

Where λ_i and I_i are the are the wavelength and intensity at *i*, respectively. Average wavelength data were normalized for comparison. LCs do not refold fully reversibly from urea (1), so we cannot report free energies of unfolding. Midpoint urea concentrations were calculated by fitting the titration data to a 2-state unfolding equation:

9) $$Fraction\ folded = \frac{(a+bx)e^{\frac{G-mx}{RT}}+(c+dx)}{1+e^{\frac{G-mx}{RT}}}$$

where *x* is the urea concentration (M), *G* is the free energy of unfolding (kJ mol^{-1}), *m* is the denaturant dependence of the unfolding reaction (kJ mol^{-1} M^{-1}), *R* is the ideal gas constant, *T* is the temperature in K, *a* and *c* are the fluorescence of the folded and unfolded states, and *b* and *d* are the denaturant dependence of the fluorescence of the folded and unfolded states, respectively. C_m, the midpoint concentration, is:

10) $$C_m = \frac{G}{m}$$

Aggregation

WIL C214S was dialyzed into ddH_2O and filtered. Each 1 ml reaction contained 10 µM LC, ddH_2O, 1% DMSO or 200 µM **1** in 1% DMSO, 150 mM NaCl, and ABC buffer (20 mM sodium acetate, 20 mM boric acid, 20 mM sodium citrate, pH 5 with HCl). Components are listed in the order they were added.

For analysis by SEC, reactions were set up in 2 ml tubes (Axygen #SCT-200-B-S) equipped with 4 mm stir bars. For each experiment, four reactions (two replicates each of vehicle and **1**) were placed in a microfuge tube rack on top of the center of a stir plate. Reactions were stirred at approximately 2,000

rpm at 37 °C, and 60 µl aliquots were removed at the indicated timepoints. Aliquots were centrifuged at 16,000 g at 4 °C for 5 min. 10 µl of the supernatant was injected into a Waters Acquity H-Class Bio-UPLC (ultra performance liquid chromatography) instrument equipped with a BEH200 SEC column (Waters, Milford, MA) equilibrated with PBS with 1 mM EDTA. At the end of an experiment, stir bars were washed for at least 3 h with 1 M NaOH, followed by at least 3 h with 6 M GuHCl at room temperature to remove residual aggregates.

Thioflavin T (ThT)-containing aggregation reactions were set up in 96-well plates with similar conditions used for the reactions described above, except each 100 µl reaction also contained 2 µM ThT. Aggregation was induced with shaking as previously described (4). In total, 21 replicates for both vehicle and **1**, over four independent experiments (plates) were performed.

Electron micrographs were recorded as previously described (1) by the Scripps Research microscopy core facility.

Supplementary NMR analysis

ZZ-exchange NMR experiment for quantifying JTO-V•1 binding

Longitudinal two-spin order ZZ-exchange experiments were acquired using JTO-V samples at 0.14 mM (monomer concentration) in the presence of 0.06 mM **1**, with ZZ-mixing delays (t_{MIX}) after t_1 (^{15}N) evolution ranging from [1-50] ms (19). Analysis of the data must be done with care since the exchange timescale is relatively fast, with exchange cross-peaks visible even when t_{MIX} = 0 s (see Figure 4f of main text). Thus, exchange of magnetization occurs even during the time between the ^{15}N t_1 and ^{1}H t_2 acquisition periods. To fit the ZZ-exchange data in this particular regime both the delay during which magnetization is stored as longitudinal two-spin order (equal to t_{MIX} + 3.9 ms in our pulse sequence and

where Eq (11) below applies), and the subsequent delays (INEPT back-transfer and t_2 acquisition periods, where Eq (12) is germane) during which transverse ^{1}H magnetization is present (Figure S14, panel b) must be considered.

Since JTO-V is mainly dimeric in the absence of **1**, the following two-state model was considered:

$$\mathbf{P_2} + \mathbf{L} \underset{k_{\mathbf{P_2L}\rightarrow\mathbf{P_2}+\mathbf{L}}}{\overset{k_{\mathbf{P_2}+\mathbf{L}\rightarrow\mathbf{P_2L}}}{\rightleftharpoons}} \mathbf{P_2L}\,, \quad \mathrm{K_D} = \frac{k_{\mathbf{P_2L}\rightarrow\mathbf{P_2}+\mathbf{L}}}{k_{\mathbf{P_2}+\mathbf{L}\rightarrow\mathbf{P_2L}}}$$

The evolution of longitudinal two-spin order is described by

$$11) \qquad \frac{d}{dt}\overrightarrow{M} = -\tilde{T}_2\overrightarrow{M}$$

where $\overrightarrow{M}$ is the 1D array of all relevant spin operators,

$$\overrightarrow{M} = \left[\mathbf{P_2}(z), \mathbf{P_2L}(z)\right]^+$$

with the superscript + denoting transpose and $\tilde{T}_2$ is the 2x2 square Liouvillian matrix that includes terms for the relaxation of two-spin order (R_{1ZZ}) and chemical exchange contributions

$$\tilde{T}_2 = \begin{bmatrix} R_{1zz} + k_{\mathrm{AB}} & -k_{\mathrm{BA}} \\ -k_{\mathrm{AB}} & R_{1zz} + k_{\mathrm{BA}} \end{bmatrix} \quad ,$$

where k_{AB} and k_{BA} are pseudo first order rates, with A=**P₂** and B=**P₂L**. These 2 rates are related to microscopic rate constants for the two-state model, as follows:

$k_{\mathrm{AB}} = k_{\mathbf{P_2}+\mathbf{L}\rightarrow\mathbf{P_2L}} \cdot [\mathrm{L}]$ and

$k_{\mathrm{BA}} = k_{\mathbf{P_2L}\rightarrow\mathbf{P_2}+\mathbf{L}}$,

where [L] is the equilibrium concentration of free ligand.

The evolution of transverse ^{1}H magnetization following the ZZ-exchange delay is described by the relation

12) $$\frac{d}{dt}\vec{M} = -\tilde{T}_4\vec{M} \quad ,$$

where $\vec{M}$ is the 1D array of all relevant spin operators

$$\vec{M} = \left[\mathbf{P_2}(x), \mathbf{P_2}(y), \mathbf{P_2L}(x), \mathbf{P_2L}(y)\right]^+$$

and the 4x4 Liouvillian matrix $\tilde{T}_4$ contains ^{1}H transverse relaxation elements and chemical shift values ($\tilde{\mathrm{P}}_4$), and chemical exchange contributions ($\tilde{K}_2 \otimes \tilde{I}_2$, where $\tilde{I}_2$ is the 2x2 identity matrix)

$$\tilde{T}_4 = \tilde{\mathrm{P}}_4 + \tilde{K}_2 \otimes \tilde{I}_2 \,, \quad \tilde{\mathrm{P}}_4 = \begin{bmatrix} \tilde{\mathrm{P}}_2^{\mathbf{P_2}} & 0 \\ 0 & \tilde{\mathrm{P}}_2^{\mathbf{P_2L}} \end{bmatrix}.$$

The $\tilde{\mathrm{P}}_2^i$ matrices describe relaxation and evolution of the spin operators for each state *i*, for *i* in [**P$_2$**, **P$_2$L**],

$$\tilde{\mathrm{P}}_2^i = \begin{bmatrix} R_2^i & \omega^j \\ -\omega^j & R_2^i \end{bmatrix}$$

while the $\tilde{K}_2$ matrix describes pseudo first-order chemical exchange

$$\tilde{K}_2 = \begin{bmatrix} k_{\mathrm{AB}} & -k_{\mathrm{BA}} \\ -k_{\mathrm{AB}} & k_{\mathrm{BA}} \end{bmatrix},$$

where k_{AB} and k_{BA} are defined as for Eq (11). To simulate chemical exchange during t_2, a 0.8 s FID was generated using Eq (12) and subsequently converted to the frequency domain by Gaussian apodization and Fourier transformation.

The parameters in the model are:

Parameter	Note
ϖ^{P_2}	Set to the negative of half of the difference in ^{1}H chemical shifts between the two exchanging states
ϖ^{P_2L}	Set to - ϖ^{P_2}
$R_{1ZZ}^{P_2} = R_{1ZZ}^{P_2L}$	Fitting parameter with fitted value of 10.7 ± 0.4 s^{-1}
$R_2^{P_2} = R_2^{P_2L}$	Fitting parameter with fitted value of 45 ± 6 s^{-1}
$K_D = \frac{k_{P_2L \rightarrow P_2+L}}{k_{P_2+L \rightarrow P_2L}}$	Fitting parameter with fitted value of 57 ± 4 µM
$k_{P_2L \rightarrow P_2+L}$	Fitting parameter with fitted value of 57 ± 2 s^{-1}

A plot of the reduced chi-square, $\chi^2_{RED.}$, for the fit *vs* K_D is shown in Figure S11, panel c, with a well-defined minimum around the best-fit K_D value.

CEST NMR experiment for WIL-V•1 binding

^{15}N-CEST experiments were acquired on WIL-V samples at 0.4 mM (monomer concentration) in the presence of 0.17 or 0.34 mM **1** using a multi-site excitation scheme recently proposed by Yuwen et al. (20) The CEST profile of Y36 (Figure S14, panel d) was chosen for analysis because only a single ^{15}N resonance is observed for the bound state, simplifying data-fitting and extraction of an apparent K_D. Since this protein is mainly monomeric in the absence of **1**, a three-state model must be considered in the interpretation of the data,

$$2\mathbf{P} \underset{k_{\mathbf{P_2}\rightarrow 2\mathbf{P}}}{\overset{k_{2\mathbf{P}\rightarrow \mathbf{P_2}}}{\rightleftharpoons}} \mathbf{P_2}$$

$$\mathbf{P_2}+\mathbf{L} \underset{k_{\mathbf{P_2L}\rightarrow \mathbf{P_2}+\mathbf{L}}}{\overset{k_{\mathbf{P_2}+\mathbf{L}\rightarrow \mathbf{P_2L}}}{\rightleftharpoons}} \mathbf{P_2L}, \quad \mathrm{K_D} = \frac{k_{\mathbf{P_2L}\rightarrow \mathbf{P_2}+\mathbf{L}}}{k_{\mathbf{P_2}+\mathbf{L}\rightarrow \mathbf{P_2L}}}.$$

The Bloch-McConnell equations (21) describing the evolution of magnetization from chemical exchange and relaxation can be written as

$$\frac{d}{dt}\vec{M} = -\tilde{T}_9\vec{M}, \qquad 13)$$

where $\vec{M}$ is the 1D array of all relevant spin operators

$$\vec{M} = \left[\mathbf{P}(x), \mathbf{P}(y), \mathbf{P}(z), \mathbf{P_2}(x), \mathbf{P_2}(y), \mathbf{P_2}(z), \mathbf{P_2L}(x), \mathbf{P_2L}(y), \mathbf{P_2L}(z)\right]^{+}$$

and $\tilde{T}_9$ is the 9x9 square Liouvillian matrix, that includes spin relaxation, chemical shift ($\tilde{\mathrm{P}}_9$) and chemical exchange contributions ($\tilde{K}_3 \otimes \tilde{I}_3$, where $\tilde{I}_3$ is the 3x3 identity matrix):

$$\tilde{T}_9 = \tilde{\mathrm{P}}_9 + \tilde{K}_3 \otimes \tilde{I}_3, \quad \tilde{\mathrm{P}}_9 = \begin{bmatrix} \tilde{\mathrm{P}}_3^{\mathrm{P}} & 0 & 0 \\ 0 & \tilde{\mathrm{P}}_3^{\mathrm{P_2}} & 0 \\ 0 & 0 & \tilde{\mathrm{P}}_3^{\mathrm{P_2L}} \end{bmatrix}.$$

The $\tilde{\mathrm{P}}_3^i$ matrices describe relaxation (R_2, R_1) and chemical shift evolution (ω) evolution for each state *i*, for *i* in [**P**, **P₂**, **P₂L**]

$$\tilde{\mathrm{P}}_3^i = \begin{bmatrix} R_2^i & \omega^i & 0 \\ -\omega^i & R_2^i & 0 \\ 0 & 0 & R_1^i \end{bmatrix}.$$

In turn, the $\tilde{K}_3$ matrix takes into account pseudo first-order chemical exchange between the three states, where A=**P**, B=**P₂** and C=**P₂L**

$$\tilde{K}_3 = \begin{bmatrix} k_{AB} & -k_{BA} & 0 \\ -k_{AB} & k_{BA}+k_{BC} & -k_{CB} \\ 0 & -k_{BC} & k_{CB} \end{bmatrix}.$$

The 4 rates of this matrix are related to microscopic rate constants for the 3-state model, as follows:

$$k_{AB} = 2 \cdot k_{2P \to P_2} \cdot [P] \quad ,$$

$$k_{BA} = k_{P_2 \to 2P} \quad ,$$

$$k_{BC} = k_{P_2 + L \to P_2L} \cdot [L] \quad ,$$

$$k_{CB} = k_{P_2L \to P_2 + L} \quad .$$

The parameters of the model are:

Parameter	**Note**
ϖ^{P}	119.9 ppm, from the NMR spectrum in the absence of **1** (blue contours in Figure S14, panel d).
ϖ^{P_2}	Fitting parameter with fitted value of 119.6 ppm
ϖ^{P_2L}	119.5 ppm, from the NMR spectrum with excess of 1 (green contours in Figure S14, panel d).
$R_1^{P} = R_1^{P_2} = R_1^{P_2L}$	Fitting parameter with fitted value of 1.4 s^{-1}
R_2^{P}	Fitting parameter with fitted value of 39 s^{-1}
$R_2^{P_2} = R_2^{P_2L}$	Set to $R_2^{P} \cdot 1.8$. Based on $R_{1\rho}$ experiments dimerization leads to an increase of 80% in ^{15}N transverse relaxation rates.
$K_{2P \rightleftarrows P_2} = \frac{k_{P_2 \to 2P}}{k_{2P \to P_2}}$	Restrained between 1 and 10 mM. Chemical shift changes upon dilution of the protein indicate that the dissociation constant for monomer-dimer equilibrium in the absence of **1** is approximately 5 mM; therefore this parameter was restrained to be within 1 and 10 mM.

$k_{P_2 \rightarrow 2P}$	Faster than 1000 s^{-1}. ^{15}N CPMG experiments indicate that the timescale of monomer-dimer exchange in the absence of **1** is fast on the chemical shift scale ($k_{P_2 \rightarrow 2P}$ > 1000 s^{-1}). The quality of the fit and the value of the fitted K_D are rather insensitive to $k_{P_2 \rightarrow 2P}$ rates higher that 1000 s^{-1} (Figure S14, panel e).
$K_D = \frac{k_{P_2L \rightarrow P_2 + L}}{k_{P_2 + L \rightarrow P_2L}}$	Fitting parameter with fitted value of 1 μM
$k_{P_2L \rightarrow P_2 + L}$	Fitting parameter with fitted value of 1 s^{-1}

The plot of the reduced chi-square function, $\chi^2_{RED.}$, as a function of the fitted K_D value is shown in Figure S14, panel f, for 3 different values of $k_{P_2 \rightarrow 2P}$. As expected, the curves are essentially independent of $k_{P_2 \rightarrow 2P}$. The absence of a well-defined minimum in $\chi^2_{RED.}$ implies that the fitted value of 1 μM for K_D is not precise. It is the case, however, that K_D must be smaller than tens of μM.

Supplemental figures

a

```
Chothia      1          11           21            A  B31           41          51
Kabat        1          11           21          A B   31           41          51
WIL-V        MNFLLTQPHSV SESPGKTVTI SCTRSSGSIA NNYVHWYQQR PGSSPTTVIF EDDHRPSGVP
JTO-V        MNFMLNQPHSV SESPGKTVTI SCTRSSGNID SNYVQWYQQR PGSAPITVIY EDNQRPSGVP
Sequential   1           11           21           31           41          51

Chothia      61         A  B   71            81            91           101
Kabat        61       A B       71            81            91           101
WIL-V        DRFSGSVDTS SNSASLTISG LKTEDEADYY CQSYDHNNQV FGGGTKLTVL
JTO-V        DRFAGSIDRS SNSASLTISG LKTEDEADYY CQSYDARNVV FGGGTRLTVL
Sequential   61          71           81           91          101
```

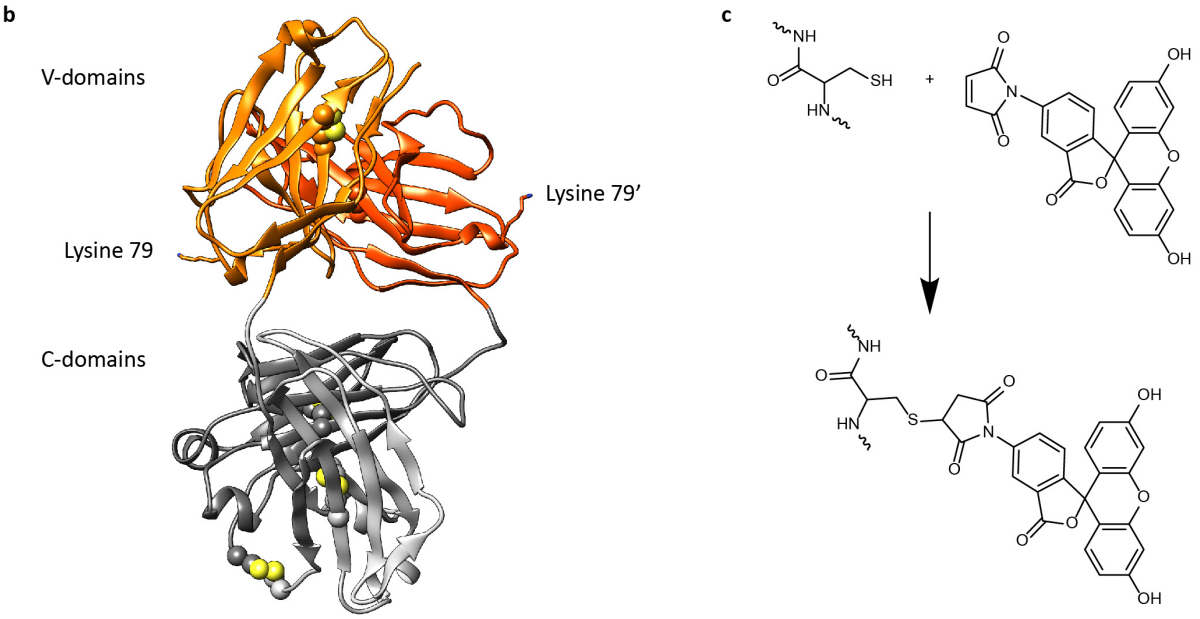

Supplemental Figure S1: LCs used in this study. a) Sequence alignment of the V-domains of WIL and JTO (22). Numbering is shown according to the Kabat and Chothia schemes; sequential residue numbering of the recombinant constructs used, which include an N-terminal methionine residue, is shown for reference. Lysine 79, which was mutated to cysteine for labeling, is highlighted. In the full-length LC constructs, the V-domains are fused to the λC3 constant domain. b) Crystal structure of dimeric JTO-FL. V-domains are shown in orange, C-domains are shown in grey, and disulfide bonds are shown as spheres. c) Labeling of cysteine 79 with fluorescein maleimide.

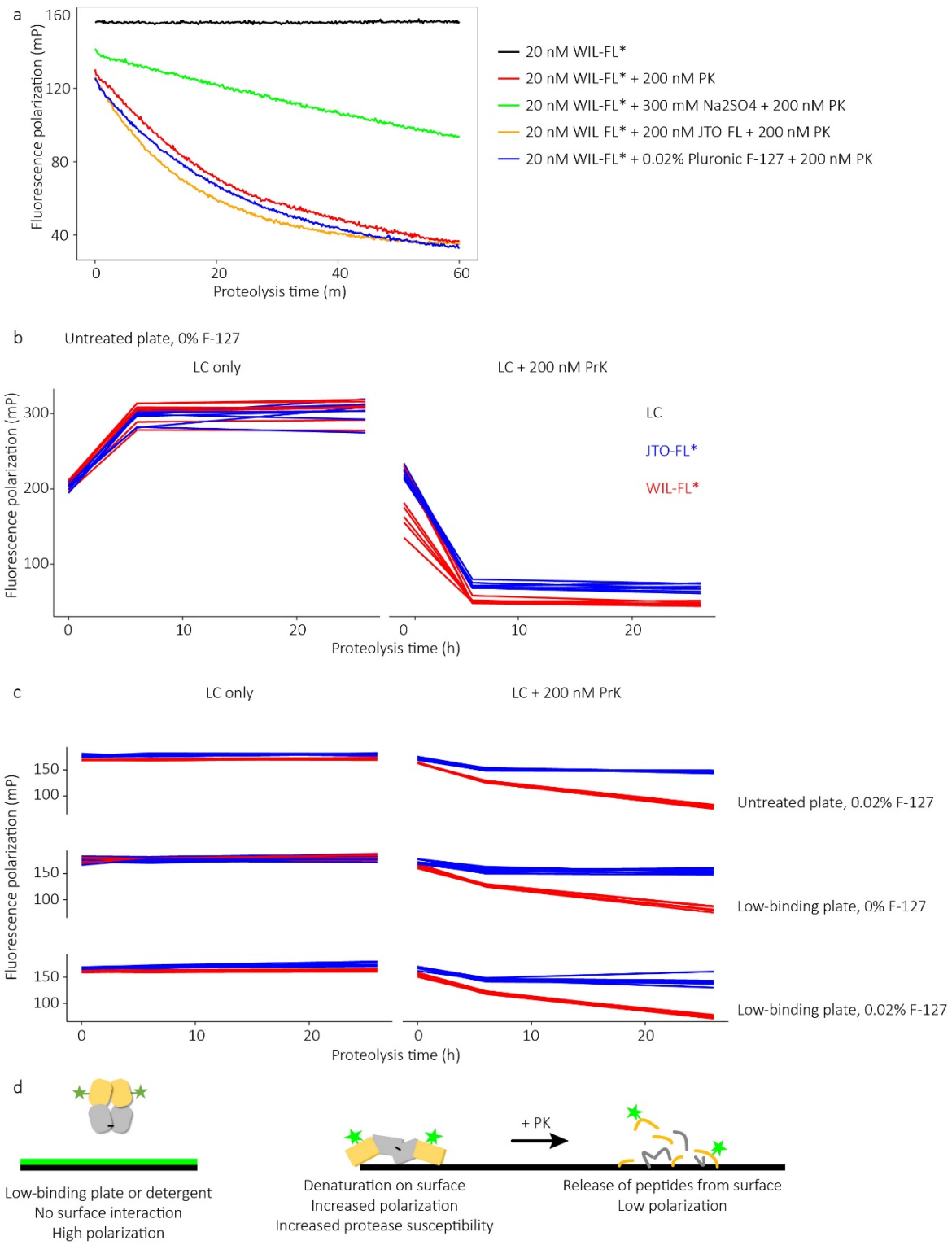

Supplemental Figure S2: Addition of detergent is necessary for the PCFP assay in multi-well plates. a) Proteolysis of WIL-FL* (20 nM) at 37 °C in quartz cuvettes. Addition of Pluronic F-127 detergent (blue

line) or an excess of unlabeled JTO-FL (orange line) does not change the rate of WIL-FL* proteolysis. Addition of 300 mM Na_2SO_4 (green line) reduces the rate of WIL-FL* proteolysis consistent with stabilization of the LC by this kosmotropic salt. b) Change in FP after incubation of WIL-FL* (20 nM; red lines) or JTO-FL* (20 nM; blue lines) in the presence or absence of 200 nM PK on 96-well plates, n=8. On untreated plates (Greiner #655076) similar to those used for the screen, FP increases in the absence of PK, and the apparent rate of proteolysis of WIL-FL* and JTO-FL* are indistinguishable. Note that our initial experiment measured the endpoint FP of WIL-FL* with and without PK, and so did not identify this problem. Kinetic experiments and the comparison with JTO-FL* were necessary to achieve a working assay. c) On low-binding plates (Corning #3651) or in the presence of 0.02% Pluronic F-127 detergent, FP decreases only in the presence of PK (compare left panels with right panels), and WIL-FL* FP decreases more rapidly than JTO-FL* FP (compare red and blue lines). The change in polarization of amyloidogenic WIL-FL* (decreases significantly with PK) and non-amyloidogenic JTO-FL* (decreases slightly with PK) is identical in low binding plates in the presence and absence of 0.02% F-127 detergent, demonstrating that the detergent is not interfering with the linked conformational changes and PK-mediated proteolysis that is central to the functionality of the high-throughput screening assay. We chose to add 0.02% F-127 detergent to untreated plates for the high-throughput screen, rather than use low-binding plates. Purchase of around 1000 barcoded plates with a non-standard surface treatment would have added significant cost to our screen. Untreated plates in combination with 0.02% F-127 detergent are widely used for high-throughput screens. d) We attribute this effect to binding of LC to the plate surface, which initially increases FP but also denatures the LC, thereby enabling more rapid proteolysis.

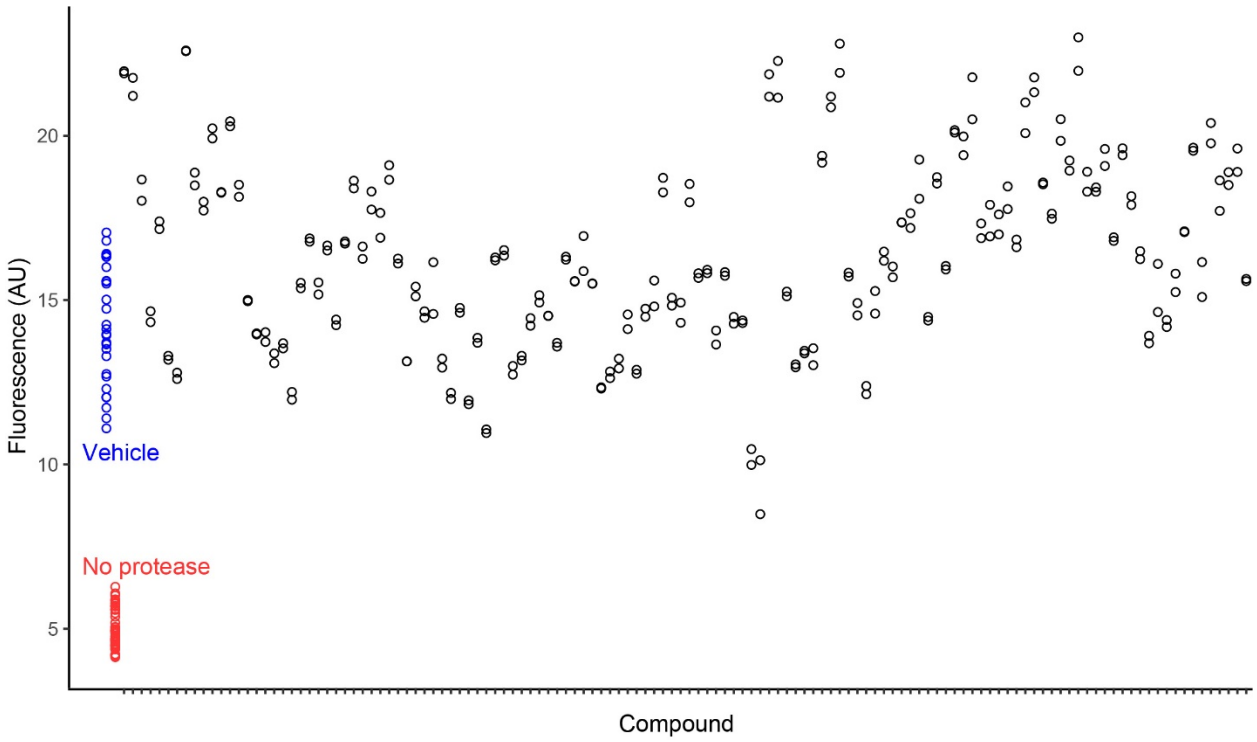

Supplemental Figure S3: Protease inhibition assay to confirm the activity of hits from the screen. Proteinase K was incubated with putative kinetic stabilizers, after which EnzCheck protease substrate was added. Cleavage of the substrate results in an increase in fluorescence. Small molecules did not inhibit proteolysis relative to vehicle (blue symbols) and negative control (no protease, red symbols).

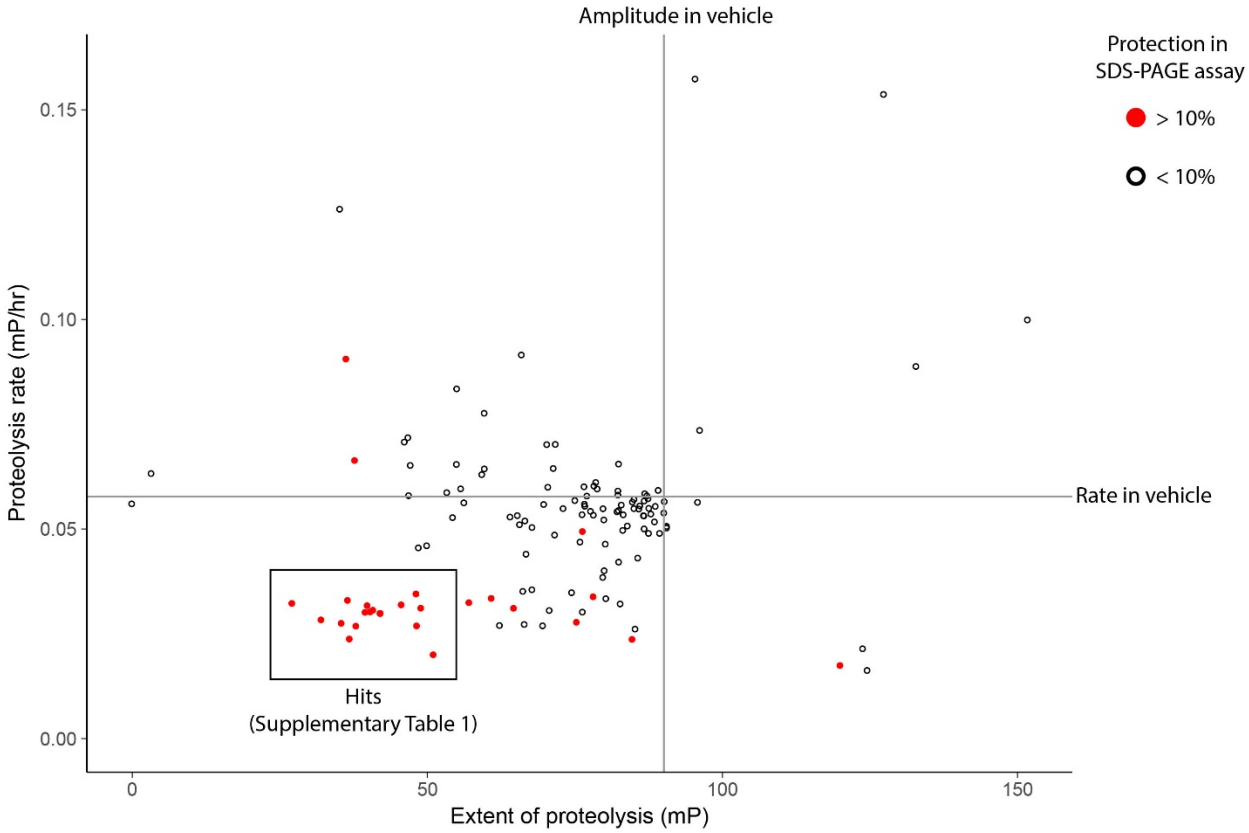

Supplementary Figure S4: PCFP kinetics and SDS-PAGE assays identify hit compounds. WIL-FL* (20 nM) was incubated with candidate molecules (6.25 µM) and PK (250 nM) for 48 h at 22°C and FP measurements were recorded at intervals. Mean (n=3) rates and amplitudes extracted from single exponential fits to the kinetic proteolysis data. Data for WIL-FL* in presence of 0.5% DMSO are shown as lines. Molecules in the lower-left quadrant of the graph are reducing the rate and amplitude of LC proteolysis, consistent with kinetic stabilization. In parallel, protection of WIL-FL* (50 nM) from proteolysis was measured using an SDS-PAGE assay (50 µM small molecule, 1 hr proteolysis, 37 °C). Small molecules that protected LCs by >10% compared to vehicle are shown as red symbols. The molecules within the box (SI Appendix Table S1) were considered hits and representative structures were selected for further analysis.

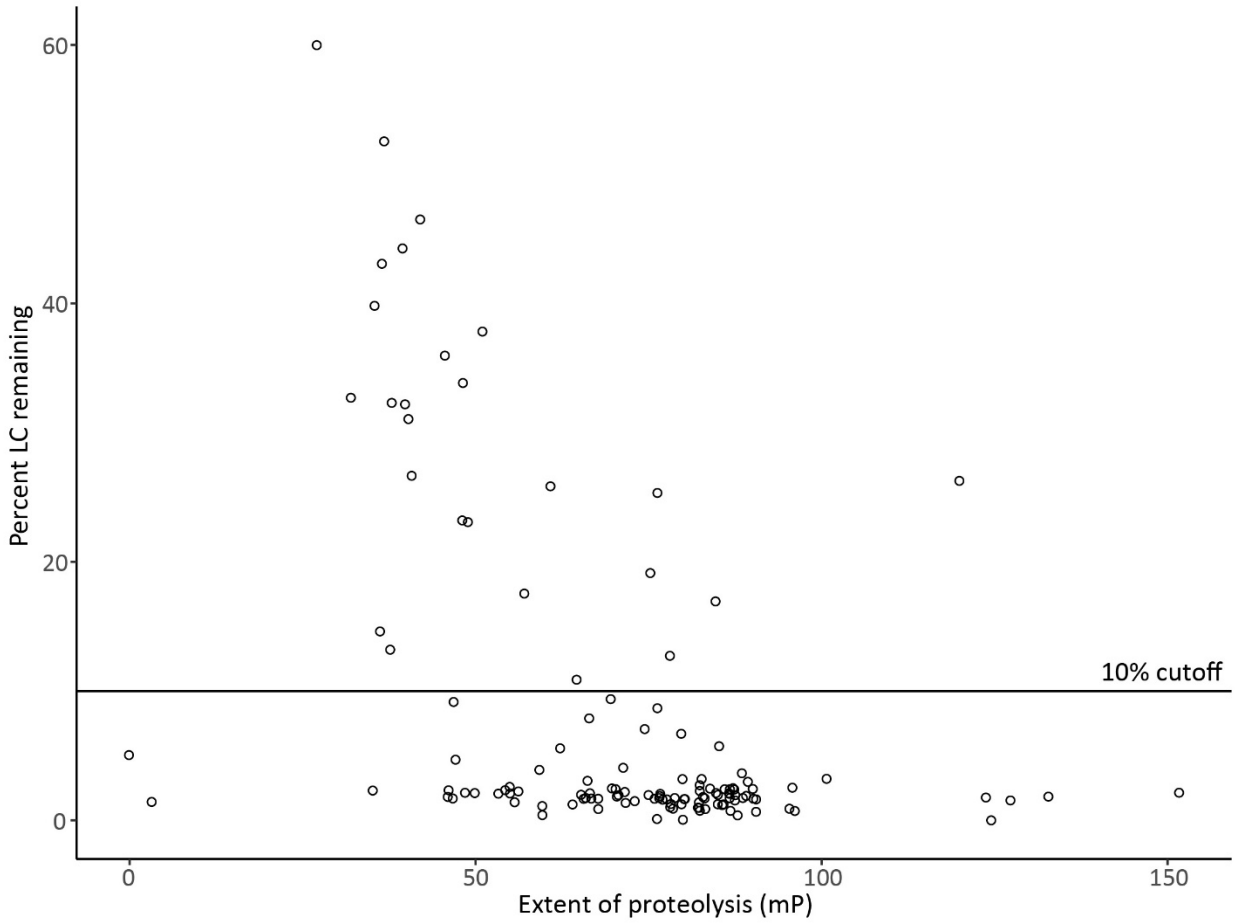

Supplementary Figure S5: Rates of proteolysis determined by SDS-PAGE and PCFP assays are correlated. Data from Supplementary Figure S4 plotted to show the correlation between protection from proteolysis as measured by SDS-PAGE and the PCFP kinetic assay, for compounds active in both assays. The 10% threshold used to define activity in the SDS-PAGE assay is shown.

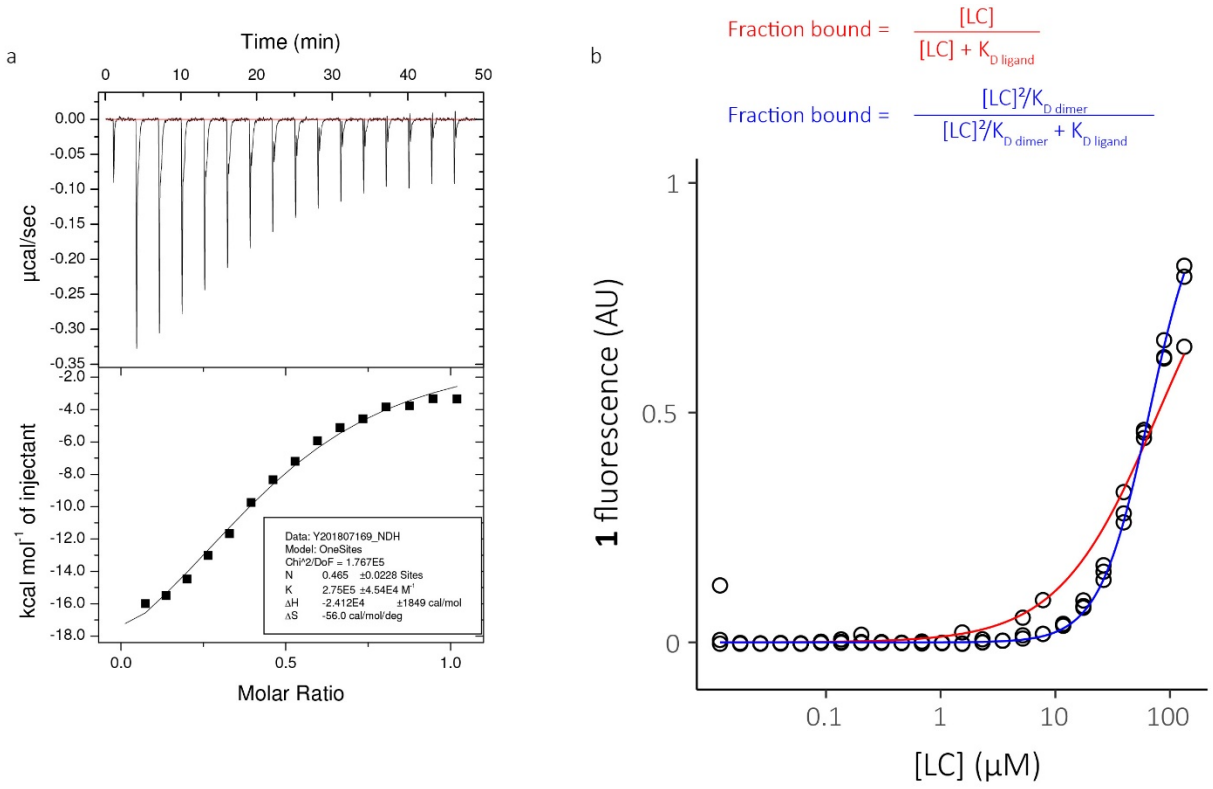

Supplementary Figure S6: Binding of **1** to LCs. a) Example ITC thermogram for sequential addition of **1** to WIL-FL. The mean K_D value from 3 replicates was 3.08 ± 0.52 µM. The stoichiometry of 0.5 indicates that a single molecule of **1** is bound by each LC dimer. b) Fits of WIL-V•**1** binding to 2-state (red) and 3-state (blue) models. Fitting to the 2-state model yields an apparent $K_{D\ ligand}$ of 79.3 ± 5.2 µM (mean + sd of 3 independent titrations). Fitting to the 3-state model constrained by the $K_{D\ dimer}$ of 5 mM measured by NMR (SI Appendix Table S2) yields an apparent $K_{D\ ligand}$ of 3.0 ± 1.2 µM.

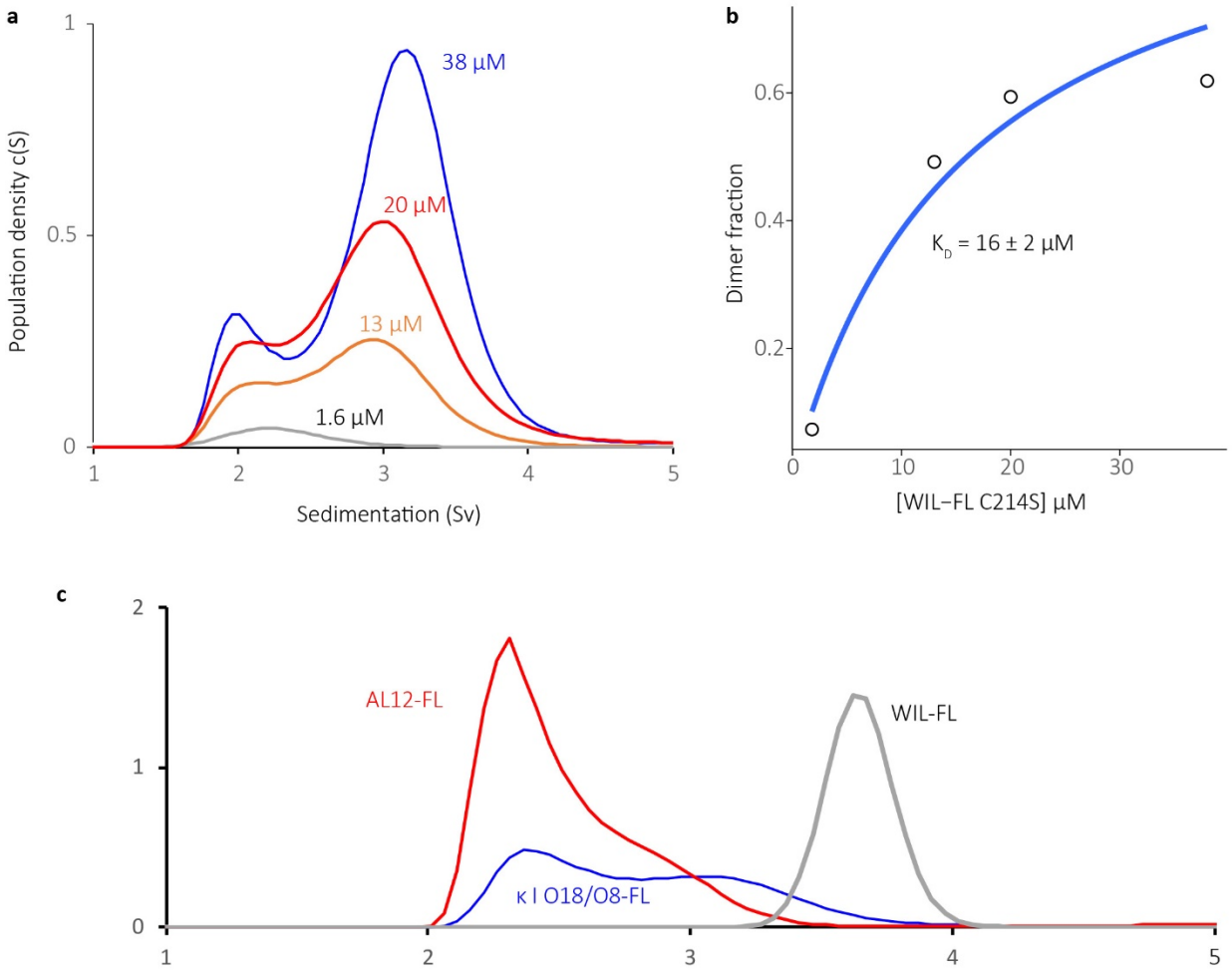

Supplementary Figure S7: Full-length LCs lacking an inter-chain disulfide bond equilibrate between monomer and dimer as observed by AUC. a) SV-AUC continuous c(S) distribution models of WIL-FL C214S at different concentrations in PBS containing 1% ethanol vehicle, pH 7.4, 20 °C. b) Quantitation of the data in a) using a 2-species model yields dimer fractions, which were fit to a dimerization model to yield a K_D of 16 ± 2 µM. c) SV-AUC continuous c(S) distribution models of the κ1-33 LCs AL12-FL (red) and κ I O18/O8-FL (blue) showing population of mainly monomeric species. Data for WIL-FL are shown for comparison in gray.

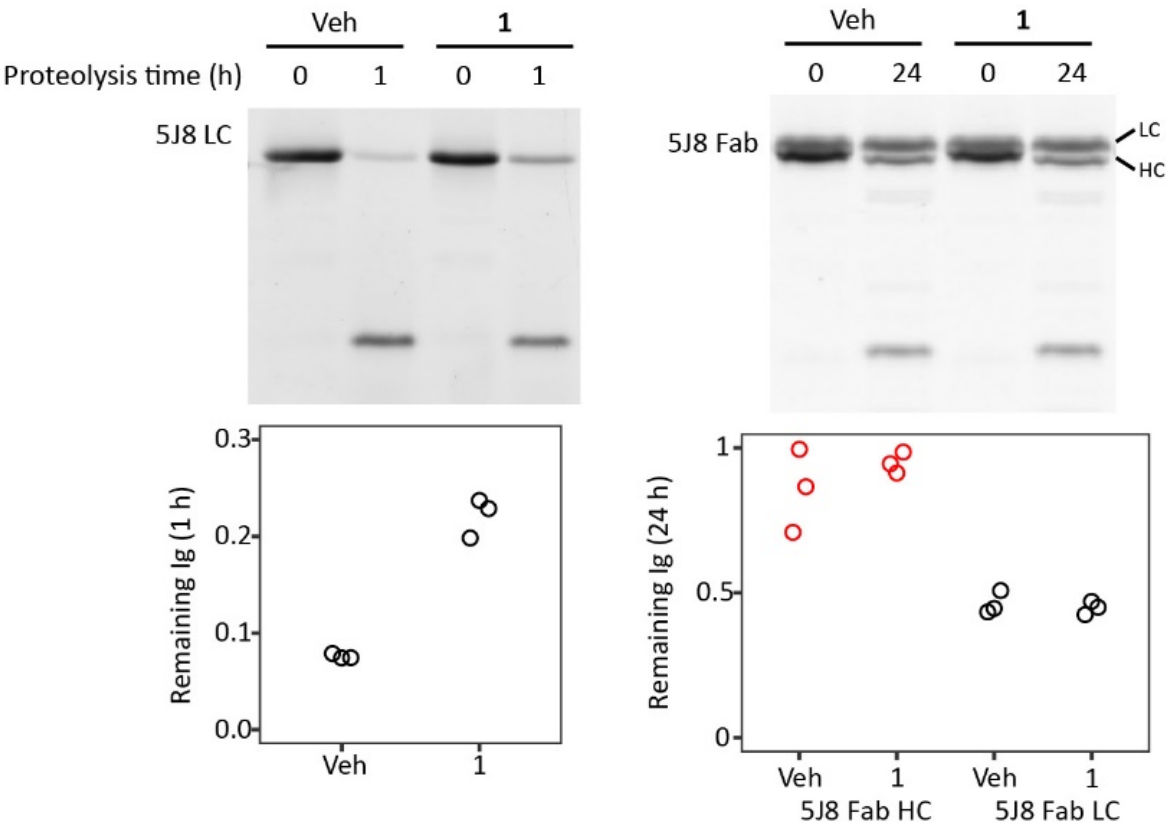

Supplementary Figure S8: Specificity of **1** for LCs over Fabs. The full-length 5J8 LC homodimer (5 µM dimer; left) or 5J8 LC:HC antigen binding fragment (Fab) heterodimer (5 µM dimer; right) were incubated with proteinase K in the presence or absence of **1** (100 µM) for 1 h (LC) or 24 h (Fab). Compound **1** protects the LC, but not the more stable Fab, from proteolysis.

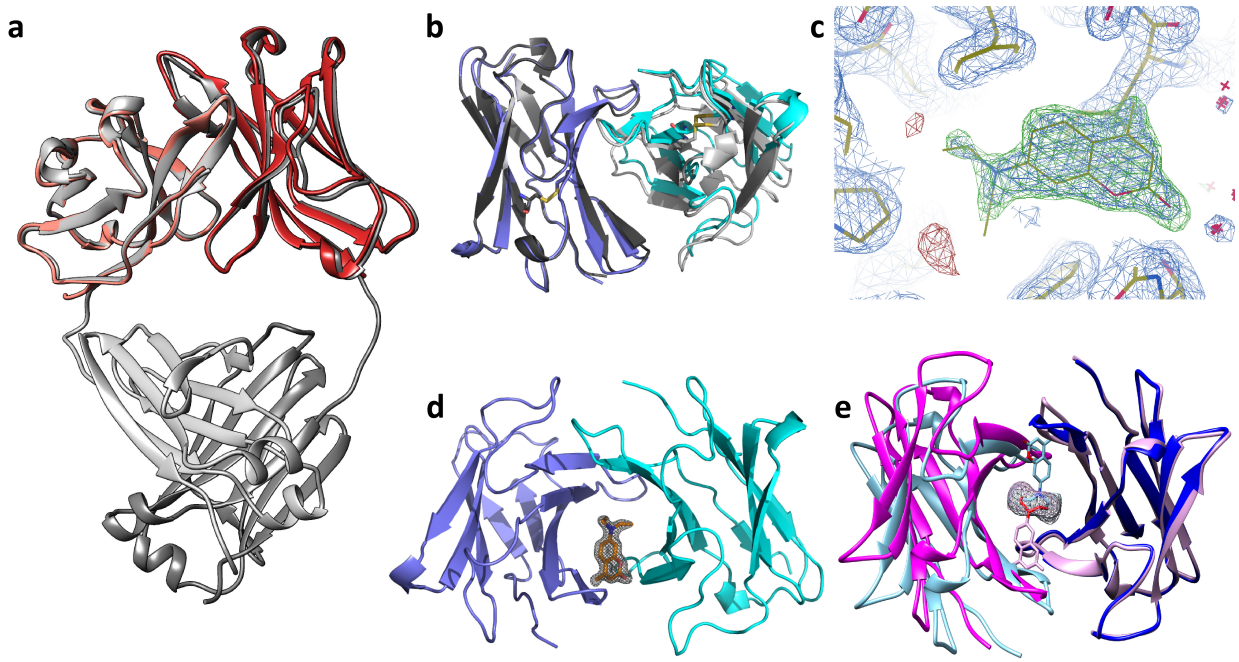

Supplementary Figure S9: a) Alignment of the published crystal structure of JTO-V (PDB: 1CD0, red) (23) with *apo* JTO-FL (grey). JTO-FL V-domains have the same arrangement in the crystal structure of the isolated V-domain as in the full-length LC. b) Rotation of V-domains to accommodate **1**. V-domain regions from the full-length structures are aligned on one domain. Disulfide bonds are shown to orient the structures. c) Electron density maps support the presence of **1** in crystal structure of JTO-FL•**1** complex. 2Fo-Fc (blue), positive Fo-Fc (green), and negative Fo-Fc (red) maps of the **1** binding site, with the ligand modeled. 2Fo-Fc and Fo-Fc density were contoured at ± 1.5 σ and ± 3.5 σ, respectively. d) "Top" view of the JTO-FL•**1** complex, showing 2Fo-Fc density around **1**. e) Binding of two molecules of **1** to JTO-FL would result in a steric clash. Superposition of two copies of the JTO-FL•**1** complex, shown as blue and purple ribbon representations, where protomer 1 (darker colors) is aligned with protomer 2 (lighter colors) to simulate the position of a second bound ligand. Clashing density is indicated by a mesh surface.

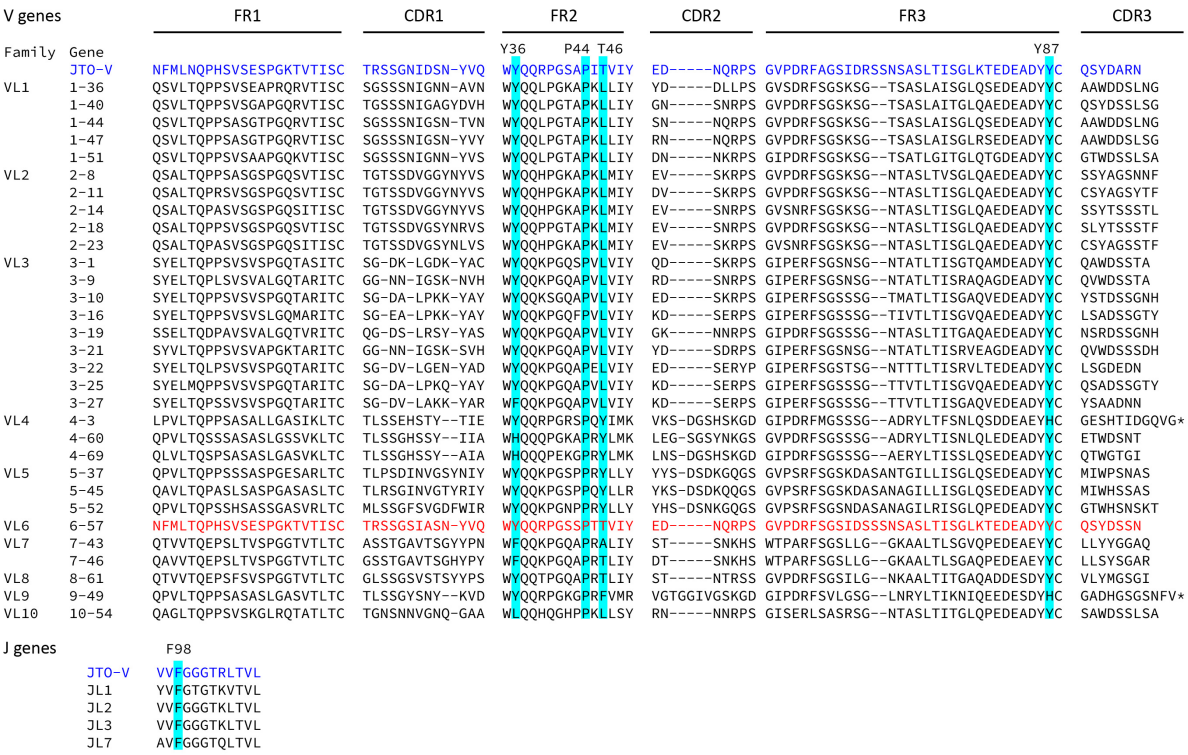

Supplementary Figure S10: Small molecule binding residues in JTO-FL are conserved. Sequence alignment of human λ LC V and J germline genes showing conservation of residues Y36, P44, Y87 and F98. The sequence of JTO-V is shown in blue and that of its parent germline gene, VL6-57, also known as λ6a, is shown in red.

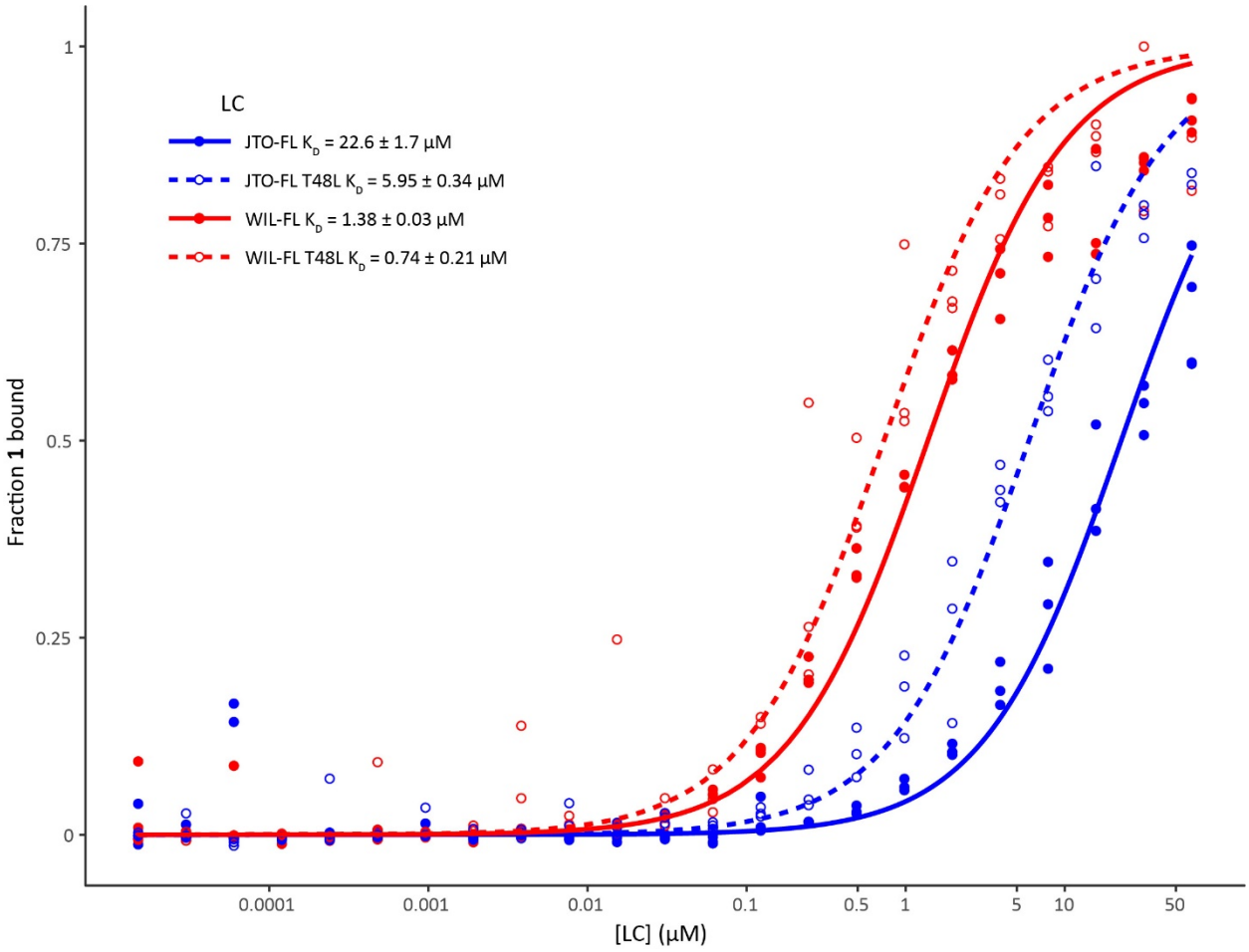

Supplementary Figure S11: Mutation of threonine 46 to leucine results in increased affinity for **1**. LCs were serially diluted 1.5-fold from 50 µM to 7 nM in PBS containing 1 µM **1** and 0.02% Pluronic F-127 detergent at ambient temperature (22 °C) on 384-well plates. Fluorescence of **1** (λ_{ex} = 373 nm, λ_{ex} = 445 nm) was measured and the fraction of **1** bound calculated. Data were fit to a single site binding model to calculate K_D values.

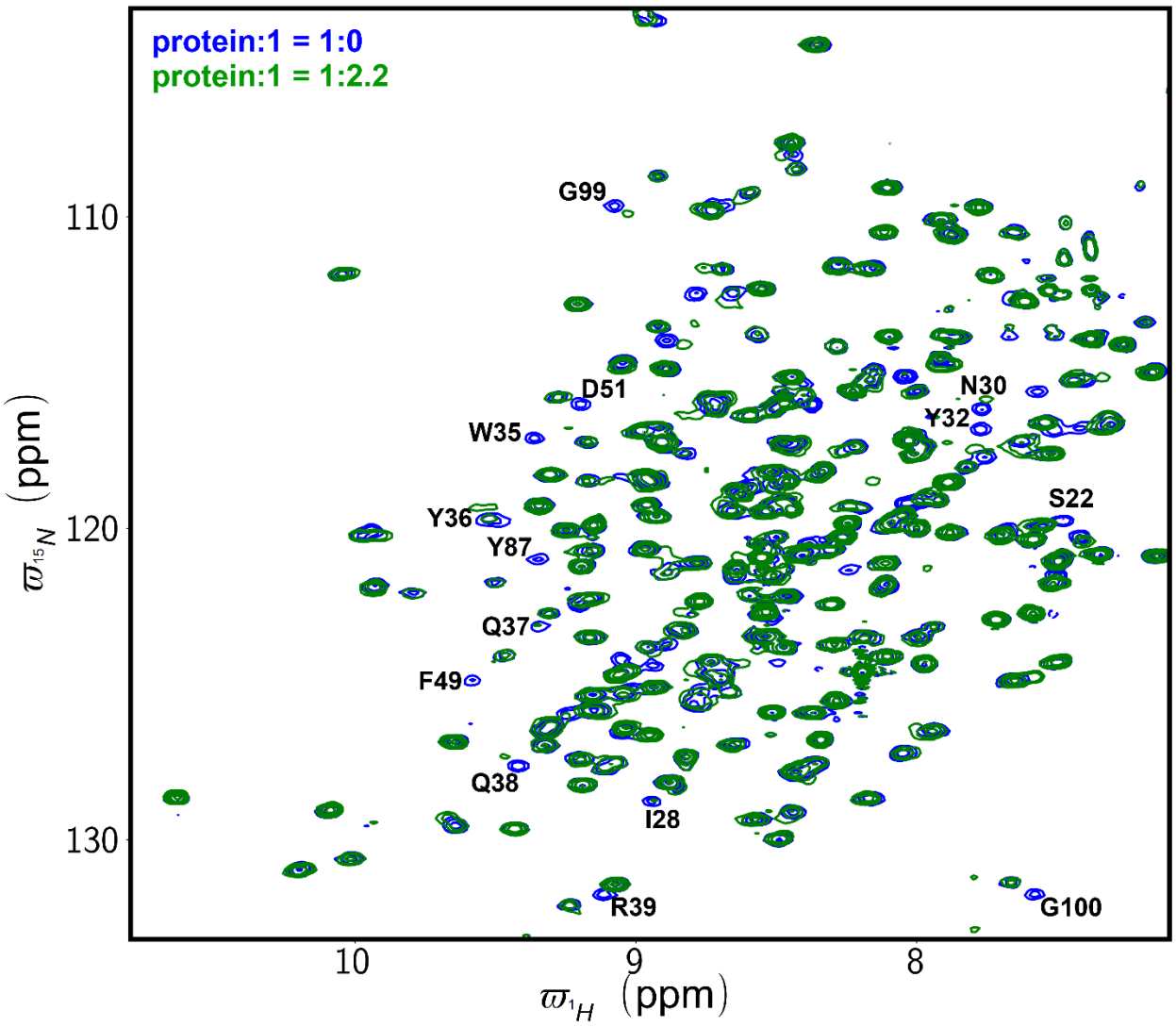

Supplementary Figure S12: Superposition of ^{1}H-^{15}N HSQC NMR spectra of WIL-FL (0.05 mM monomer equivalent concentration) in the absence (blue contours) or presence of **1** at LC:**1** ratios of 1:2.2 (green).

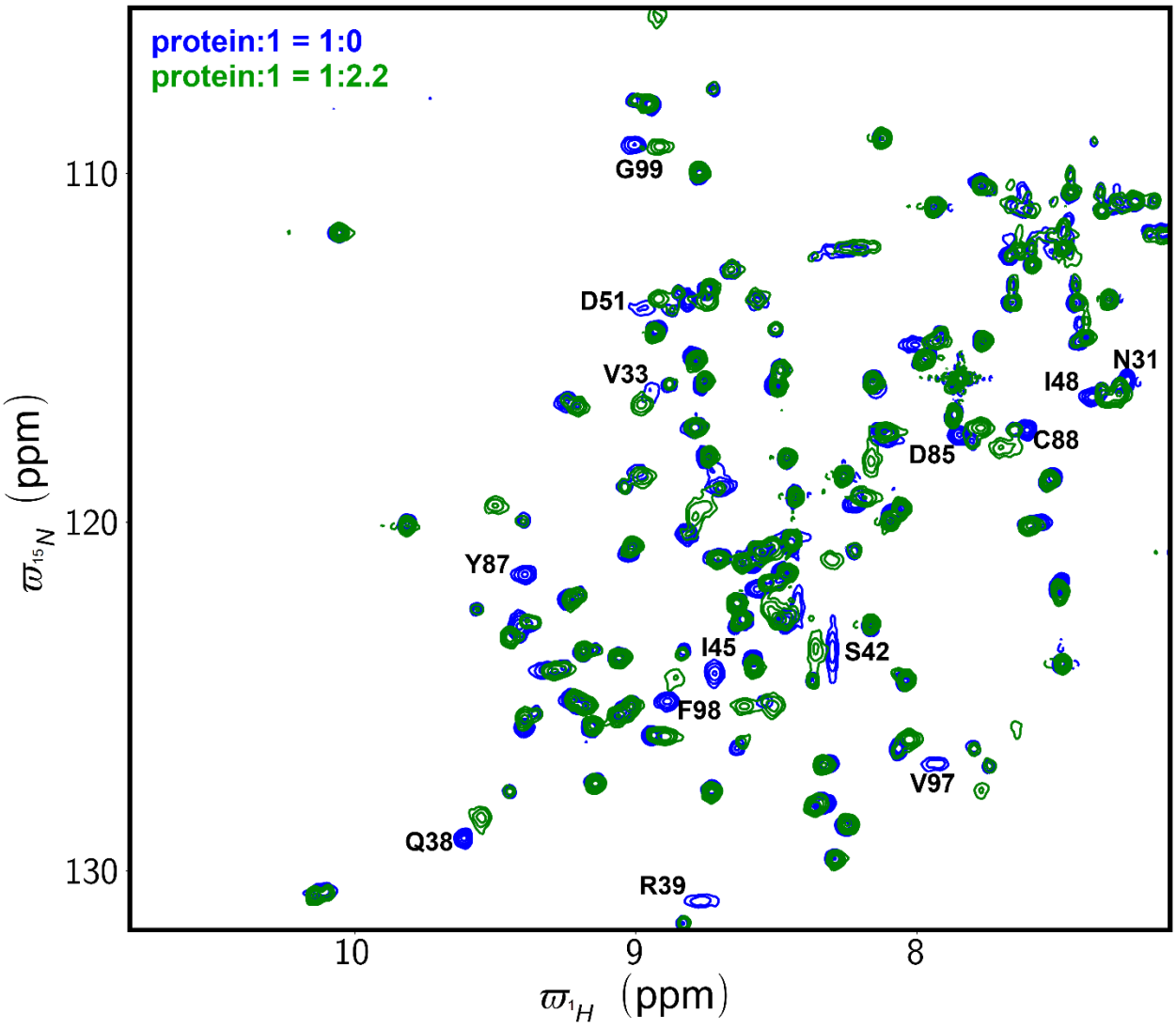

Supplementary Figure S13: Superposition of ^{1}H-^{15}N HSQC NMR spectra of JTO-V (0.14 mM) in the absence (blue contours) or presence of **1** at LC:**1** ratios of 1:2.2 (green).

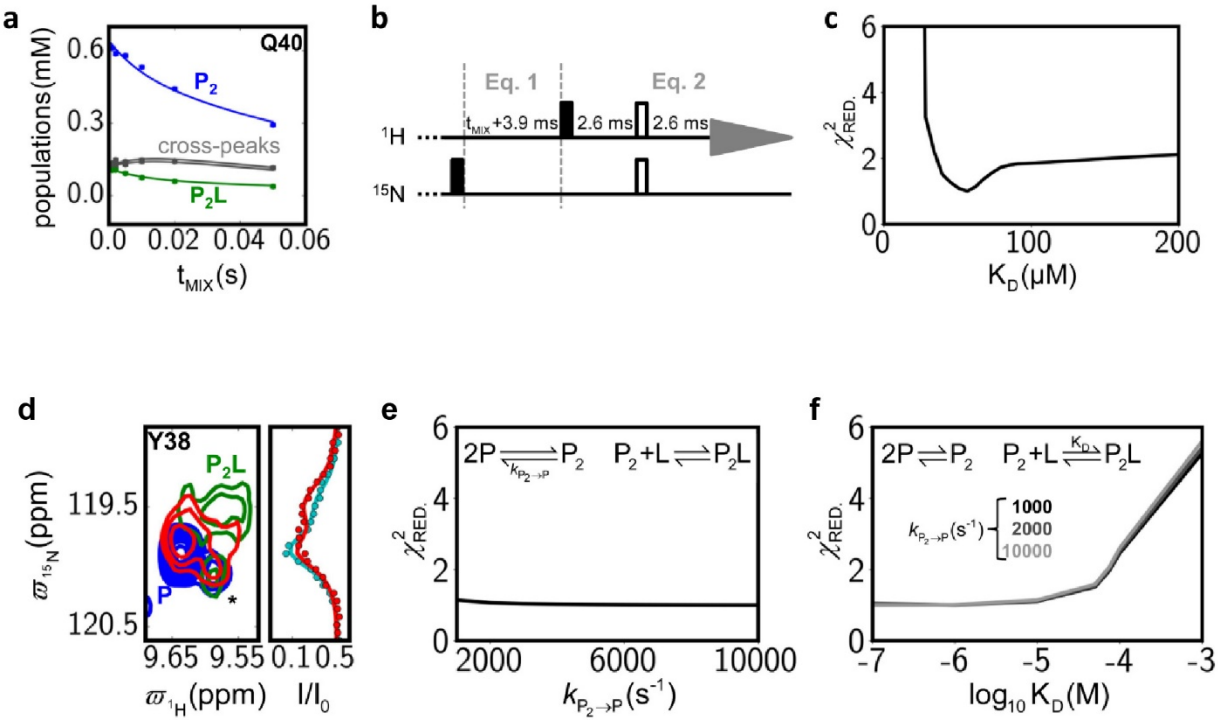

Supplementary Figure S14: Binding of **1** to LC V-domains measured by NMR. (a-c) Binding of **1** to JTO-V measured by ZZ exchange NMR experiments. a) Data points (circles) and fits (lines) for the evolution of auto-peaks and cross-peaks as a function of the mixing time. b) Scheme of the last portion of the ZZ-exchange pulse sequence, from relaxation of longitudinal two-spin order $2H_zN_z$, where **equation 11** (Supplementary NMR analysis) applies, to the last INEPT and direct acquisition time, where **equation 12** (Supplementary NMR analysis) applies. See Methods for details. c) Dependence of χ^2_{RED} on K_D. (d-f) Analysis of CEST experiment for WIL-V in the presence of **1** allows partial characterization of ligand binding. d) Left, region of ^1H,^{15}N HSQC around residue Y38, in the absence (blue) or in the presence of **1**, at WIL-V:**1** ratios of 1:0.9 (red) and 1:2.2 (green); the star indicates the position of a contaminant. Right, data points (circles) and fits (lines) of CEST profiles for Y38, in the presence of 0.17 mM (cyan) or 0.34 mM (red) **1**. The intensity of the $\mathbf{P_2}$ resonance is saturated not only when the irradiation frequency is on-resonance but also when the degenerate ^{15}N resonances of $\mathbf{P_2L}$ are irradiated. e) Dependence of χ^2_{RED}

on the timescale of monomer-dimer exchange; for these fits the fitted K_D only varies by 10%. f) Dependence of χ^2_{RED} on K_D for 3 different constrained values of $k_{P_2 \rightarrow 2P}$.

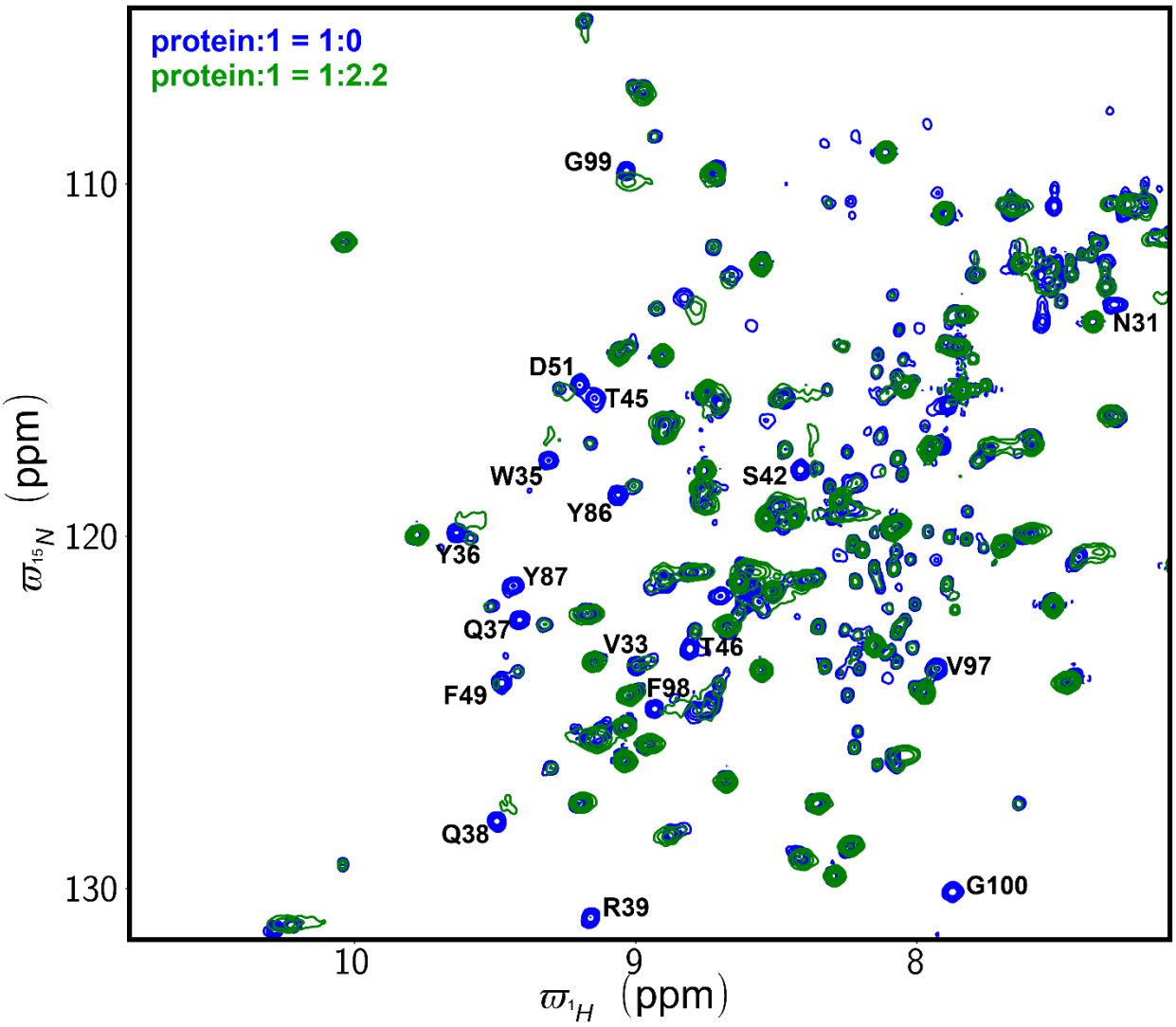

Supplementary Figure S15: Superposition of ^{1}H-^{15}N HSQC NMR spectra of WIL-V (0.4 mM) in the absence (blue contours) or presence of **1** at LC:**1** ratios of 1:2.2 (green).

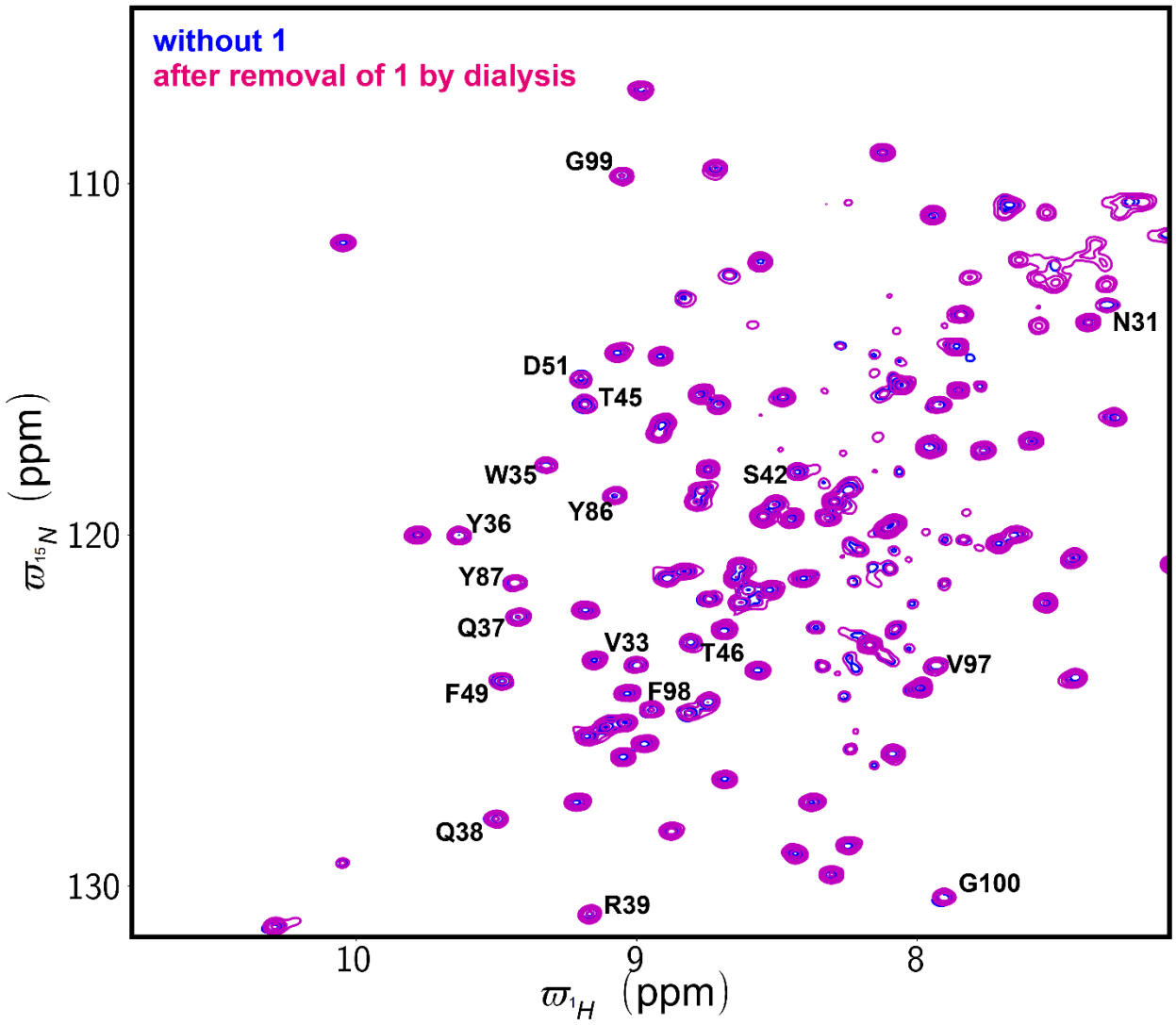

Supplementary Figure S16: Superposition of ^{1}H-^{15}N HSQC NMR spectra of two samples of WIL-V (0.025 mM): one that has never been in contact with **1** (blue contours) and the other where the ligand (at an initial LC:**1** ratio of 1:1.1) has been removed by dialysis (magenta). The equivalence between spectra acquired in the absence of **1** or after removal of the ligand by dialysis shows that binding is reversible. Furthermore, the spectra in the absence of **1** show no conformational heterogeneity; therefore, the multiple peaks observed in the presence of **1** must be attributed to multiple binding modes of the ligand.

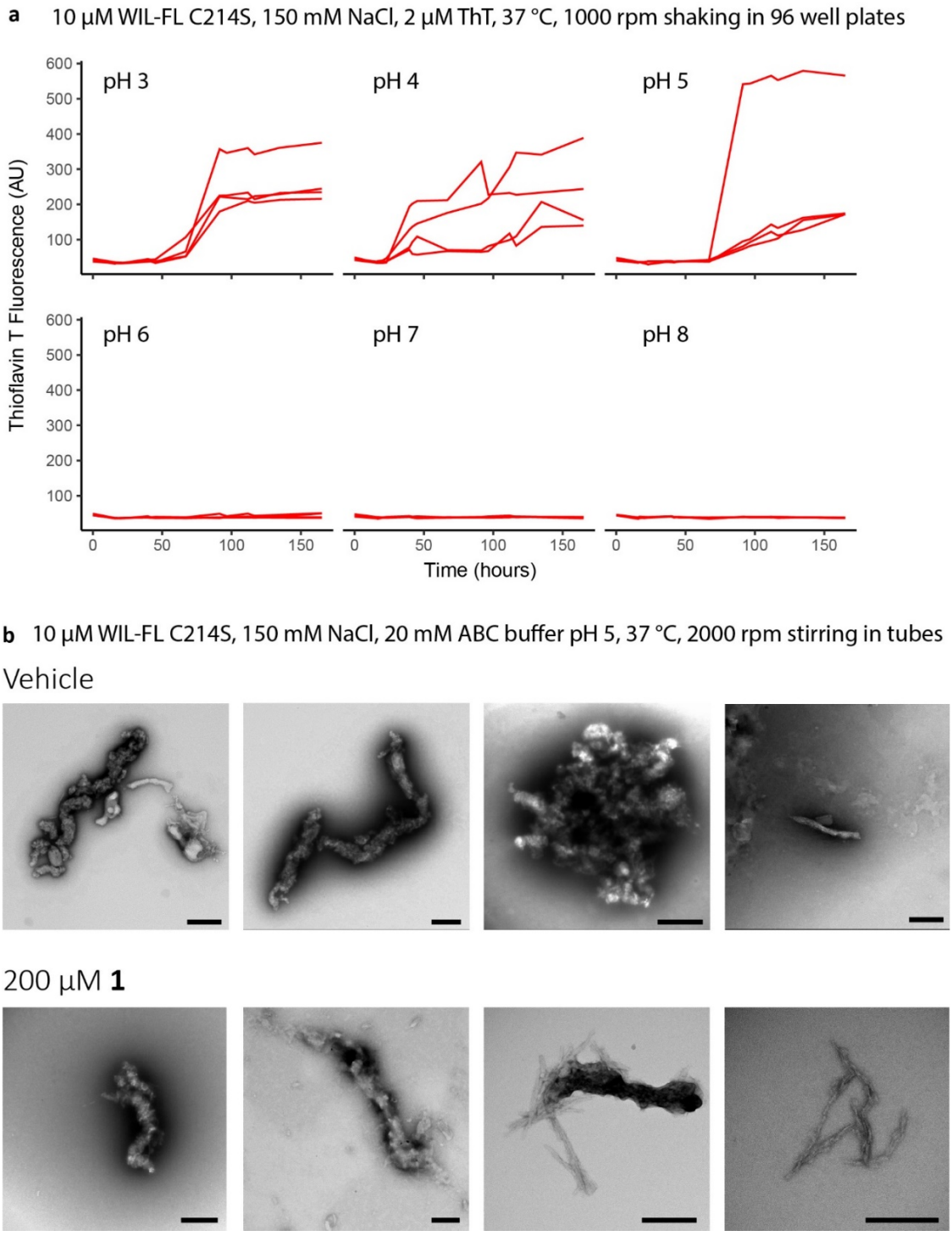

Supplementary Figure S17: WIL-FL aggregates upon agitation at or below pH 5. WIL-FL C214S was incubated in 20 mM acetate-borate-citrate (ABC) buffer (see Materials and Methods) containing 150 mM NaCl and 2 mM ThT at the pH values indicated, at 37 °C. a) pH dependence of aggregation kinetics

measured by fluorescence of the amyloid-binding dye thioflavin T (ThT, λ_{ex} = 440 nm, λ_{ex} = 480 nm). b) Electron micrographs of aggregates formed by WIL-FL C214S after 64 h incubation at pH 5, 37 °C in the presence of 1% DMSO vehicle (top) or 200 μM **1** (bottom) with vigorous stirring. Scale bars represent 0.2 μM.

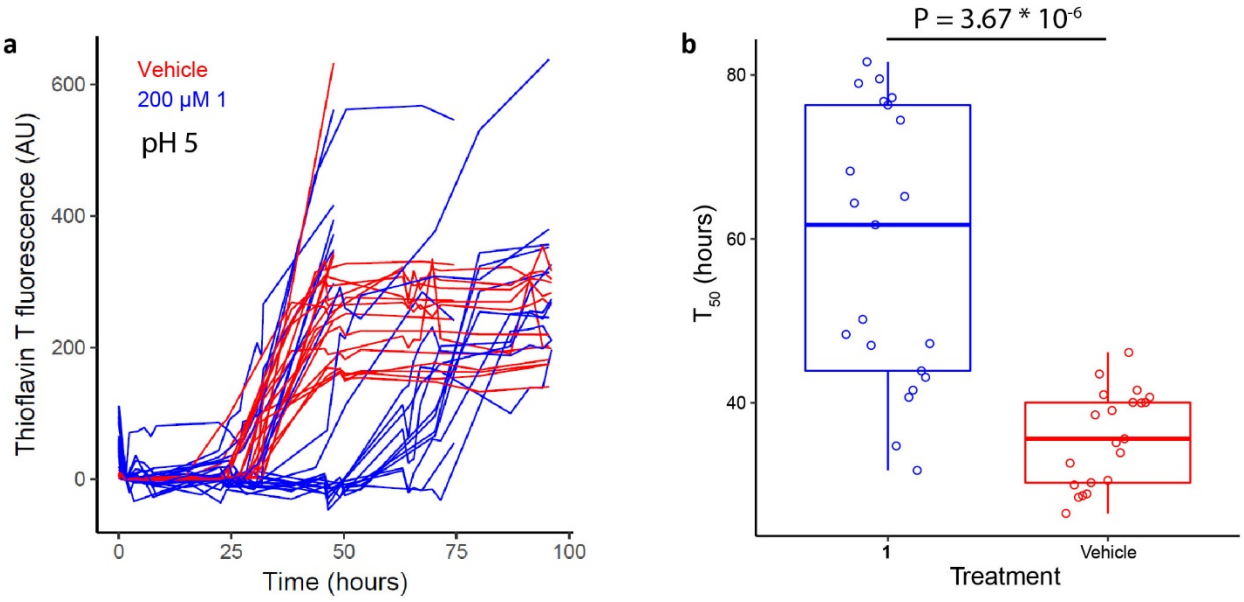

Supplemental Figure S18: Aggregation rates of WIL-FL C214S are reduced by binding of **1**. Aggregation kinetics measured by fluorescence of ThT. WIL-FL C214S was incubated in 20 mM ABC buffer containing 150 mM NaCl and 2 mM ThT at pH 5, 37 °C in the presence of 200 µM **1** (blue) or 1% DMSO vehicle (red) with shaking at 1000 rpm in 96-well plates. ThT fluorescence (λ_{ex} = 440 nm, λ_{ex} = 480 nm) was measured at intervals; buffer fluorescence was subtracted to remove the effect the fluorescence of **1**. a) Individual ThT fluorescence traces from 21 individual wells per condition, measured in four separate experiments. b) Aggregation half-times (T_{50}) calculated from the kinetic traces in (a). Boxplots show means (center lines), quartiles (boxes) and range (whiskers). Data are not normally distributed (P = 0.00010, Shapiro-Wilk normality test); P = 3.67 * 10^{-6}, 2-sided Mann-Whitney test.

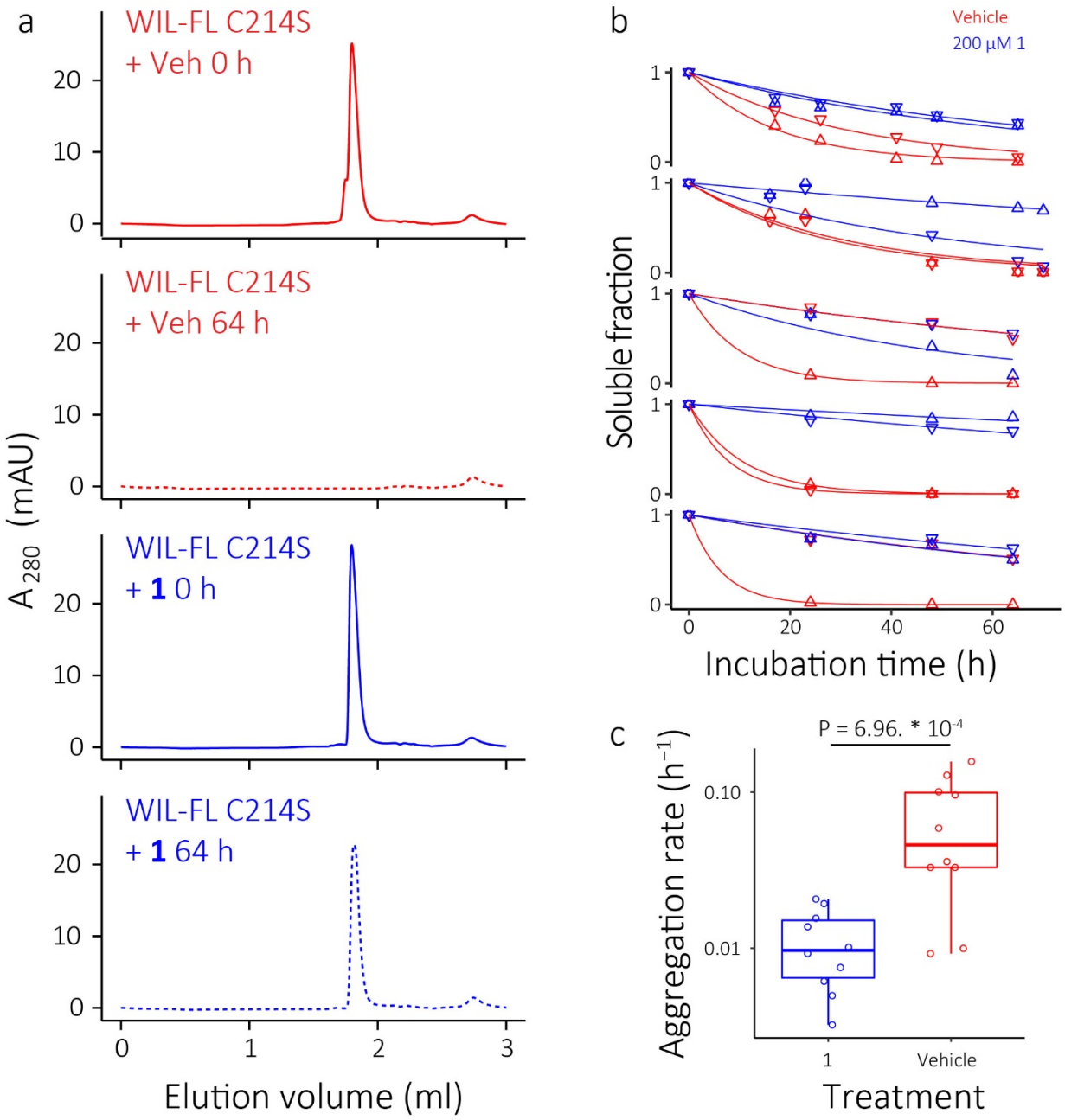

Supplemental Figure S19: Aggregation rates of WIL-FL C214S are reduced by binding of **1**. Aggregation kinetics measured by size exclusion chromatography. WIL-FL C214S was incubated in 20 mM ABC buffer containing 150 mM NaCl at pH 5, 37 °C in the presence of 200 µM **1** (blue) or 1% DMSO vehicle (red) with stirring at 2000 rpm in tubes. Aliquots were removed at intervals and centrifuged to remove aggregates. Residual soluble LC was measured by SEC. a) Example SEC traces of residual soluble LC

before (solid lines) and after (dashed lines) 64 h incubation. b) Individual data and fits to a single exponential decay model for five independent aggregation experiments, each comparing the aggregation of two samples of LC with (blue) and without (red) 200 µl **1** (10 samples per condition total). c) Rates extracted from the fits in (b). Boxplots show means (center lines), quartiles (boxes) and range (whiskers). Data are log-normally distributed (P = 0.399, Shapiro-Wilk normality test); P = 0.000696, Welch 2-sample, 2-tailed t-test on log-transformed rates.

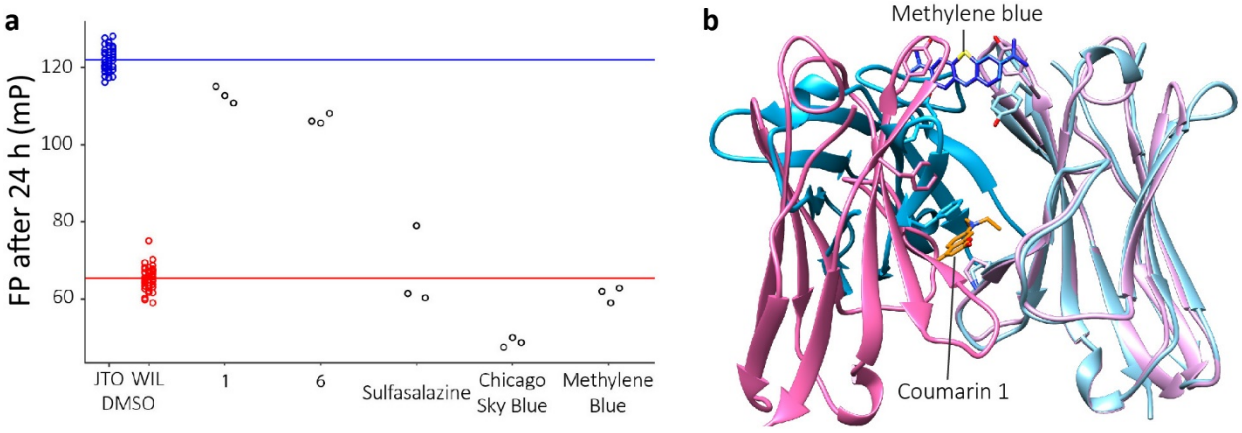

Supplemental Figure S20: Small molecules that bind to MCG-V stabilize an alternative conformation of the V-domain. a) Three small molecules identified in a screen for inhibitors of LC V-domain aggregation are inactive in the PCFP assay. Data for molecules **1** and **6** (Table 1) are shown for comparison. b) Superimposition of the structures of MCG-V (pink ribbons) bound to methylene blue (PDB 5ACM) (24) and the V-domains of JTO-FL (blue ribbons) bound to **1** show that the small molecules bind in different sites and stabilize different quaternary configurations of the LC dimer. It is not clear whether this conformation of the V-domains is accessible to the full-length LC dimer.

Supplementary Table S1: Screening data for selected small molecules that stabilize LCs and selected inactive analogs. Small molecules **1** to **16** were identified as hits from the Scripps Florida screen and showed clear activity in both the PCFP and SDS-PAGE assays. Small molecules **17** to **18** were identified as hits from the Maybridge HitFinder library. Data for the related but inactive coumarins **19**, **20** and **21** are included for reference. Activity is normalized to the activity of the high and low controls from either the pilot screen (n=1), primary screen (n=1), or counterscreen (mean ± sd, n=3). EC_{50} values are calculated from the dose response curves in SI Appendix Dataset 1. ND, not determined.

ID	CAS	Structure	PK activity (%)	Thermolysin activity (%)	Counterscreen activity (%)	EC_{50} (µM)	LC-MS validation
1	91-44-1	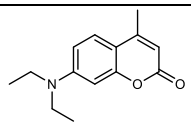	47.8±0.7	36.4±2.0	-8.07±3.3	12.5	Pass
2	107995-72-2	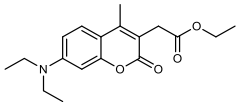	37.8±1.4	33.8±3.1	-4.13±5.2	6.92	Pass
3	332055-28-4	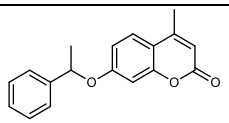	43.3±1.5	38.7±3.7	-2.52±5.8	7.1	Pass
4	402611-28-3	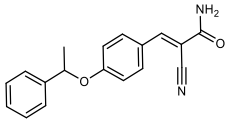	48.9±2.6	40.4±1.2	7.4±4.0	6.33	Pass
5	377766-47-7	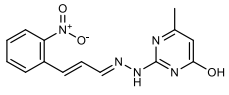	65.2±2.8	61.1±5.0	8.04±2.6	5.51	Pass
6	390779-43-8	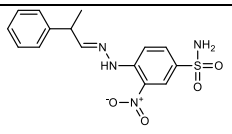	60.8±2.7	45.1±6.6	1.00±2.6	4.92	Pass

7	565443-24-5	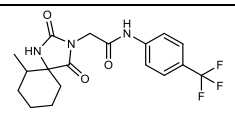	29.3±2.5	26.3±1.7	2.51±4.7	5.87	Pass
8	1008405-31-9	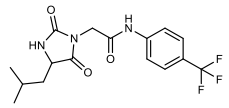	48.0±2.4	50.8±1.7	-2.05±2.9	7.36	Pass
9	20571-42-0	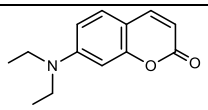	37.9±1.1	27.1±1.3	-3.45±3.89	7.9	Pass
10	115264-81-8	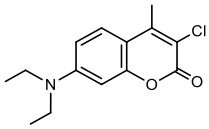	48.0±3.8	55.5±3.3	-1.54±2.4	4.0	Pass
11	107995-74-4	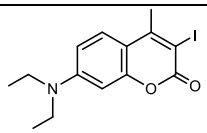	58.7±2.0	45.7±7.0	0.94±3.9	4.18	Pass
12	142878-43-1	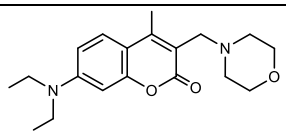	37.2±7.3	30.2±4.2	0.41±2.5	11.3	Pass
13	137501-34-9	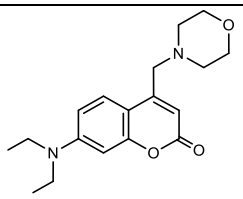	42.1±4.4	23.3±8.5	-4.10±1.5	9.15	Pass
14	107995-71-1	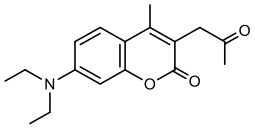	41.9±3.0	34.8±3.1	1.67±4.7	9.04	Pass
15	374701-17-4	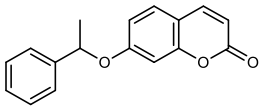	34.2±3.0	18.3±4.9	-4.35±5.6	9.28	Pass

16	500119-80-2	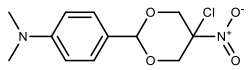	50.5±5.3	29.1±0.3	-3.09±3.0	6.73	Fail (Multiple peaks)
17	81453-98-7	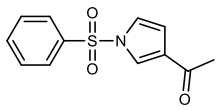	58.1 (10 µM in pilot screen)	ND	ND	18.5	ND
18	65085-83-8	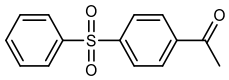	46.5 (10 µM in pilot screen)	ND	ND	18.0	ND
19	90-33-5	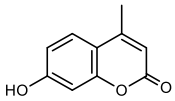	2.27 (Primary screen)	ND	ND	ND	ND
20	26093-31-2	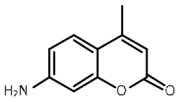	-3.02 (Primary screen)	ND	ND	ND	ND
21	91-64-5	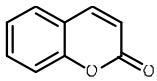	2.58 (Primary screen)	ND	ND	ND	ND

Supplementary Table S2. Summary of monomer-dimer equilibria for different LC species. Wildtype (WT) full-length λ6-57 LC constructs are obligate, disulfide-crosslinked dimers. Other species are in equilibrium between monomer and dimer. NMR measurements show that full-length, C214S LC constructs are dimeric at 200 μM. The percentage of residues at the domain interfaces between protomers which have dimer-like chemical shifts is reported. NMR data are described further in Rennella et al. (5).

LC	NMR (200 μM)	AUC (20 μM)
WT JTO-FL	Obligate dimer	Single peak 3.5 S
WT WIL-FL	Obligate dimer	Single peak 3.5 S
JTO-V	K_D = 12.5 μM	Single peak 2 S
WIL-V	K_D = 5000 μM	Single peak 1.5 S
JTO-FL C214S	100% dimer-like (V-domain interface) 93% dimer-like (C-domain interface)	Single peak 3.5 S
WIL-FL C214S	95% dimer-like (V-domain interface) 93% dimer-like (C-domain interface)	Two peaks, 2 S and 3.2 S; K_D = 16 μM
κ I O18/O8-FL	Not measured	Two peaks, 2.4 S and 3.2 S
AL12-FL	Not measured	Major peak at 2.4 S with shoulder at 2.9 S

Supplementary Table S3. Data collection and refinement statistics for crystal structures of *apo* JTO-FL and JTO-FL•**1**.

	***apo* JTO-FL**	**JTO-FL•1**
PDB code	6MG4	6MG5
Data collection		
Space group	$P2_12_12_1$	$P2_12_12_1$
(a, b, c) (Å)	63.39, 82.46, 97.02	64.07, 84.22, 96.17
(α, ß, γ) (°)	90, 90, 90	90, 90, 90
Resolution range (Å)	44.62 – 1.75 (1.78 – 1.75)	45.05 – 1.80 (1.85 – 1.80)
Unique reflections	50,814 (2,214)	47,842 (3,416)
Completeness (%)	97.5 (86.2)	98.0 (95.9)
R_{sym}	0.055 (0.49)	0.11 (1.59)
R_{pim}	0.034 (0.29)	0.051 (0.76)
CC(1/2)	0.96 (0.84)	1.00 (0.46)
I/σ (I)	18.2 (2.1)	9.5 (1.0)
Redundancy	3.5 (3.4)	5.2 (5.0)
Wilson B factor (Å^2)	28	25
Refinement		
No. atoms		
total	3,965	3,856
protein	3,301	3,336
water	664	493
ligand	0	17
Resolution range (Å)	44.66 – 1.75	45.10 – 1.80
No. reflections - work	48,204	44,684
No. reflections - free	2,560	2,312
R_{work}	0.171	0.204
R_{free}	0.222	0.263
RMS bond length (Å)	0.012	0.011
RMS bond angle (°)	1.49	1.40
Mean B value (Å^2)		
overall	39	37
protein	37	36
water	53	44
ligand	-	30
Ramachandran favored (%)	96.7	96.7
Ramachandran allowed (%)	100	100
Clashscore	3.86	1.97

Each structure was determined from one crystal. For all statistics, values in parentheses apply to reflections in the highest-resolution shell.

Supplemental References

1. Morgan GJ & Kelly JW (2016) The Kinetic Stability of a Full-Length Antibody Light Chain Dimer Determines whether Endoproteolysis Can Release Amyloidogenic Variable Domains. *J Mol Biol* 428(21):4280-4297.
2. Arendt BK*, et al.* (2008) Biologic and genetic characterization of the novel amyloidogenic lambda light chain-secreting human cell lines, ALMC-1 and ALMC-2. *Blood* 112(5):1931-1941.
3. Hong M*, et al.* (2013) Antibody recognition of the pandemic H1N1 Influenza virus hemagglutinin receptor binding site. *J Virol* 87(22):12471-12480.
4. Morgan GJ, Usher GA, & Kelly JW (2017) Incomplete Refolding of Antibody Light Chains to Non-Native, Protease-Sensitive Conformations Leads to Aggregation: A Mechanism of Amyloidogenesis in Patients? *Biochemistry* 56(50):6597-6614.
5. Rennella E, Morgan GJ, Kelly JW, & Kay LE (2018) The role of domain interactions in the aggregation of full-length immunoglobulin light chains. *Proc. Natl. Acad. Sci. USA* In press.
6. Schuck P (2000) Size-distribution analysis of macromolecules by sedimentation velocity ultracentrifugation and lamm equation modeling. *Biophysical Journal* 78(3):1606-1619.
7. Otwinowski Z & Minor W (1997) Processing of X-ray diffraction data collected in oscillation mode. *Methods in Enzymology*, (Academic Press), Vol 276, pp 307-326.
8. Kabsch W (2010) XDS. *Acta Crystallogr D: Biol Crystallogr* 66(Pt 2):125-132.
9. Evans P (2006) Scaling and assessment of data quality. *Acta crystallographica. Section D, Biological crystallography* 62(Pt 1):72-82.
10. Brünger AT (1992) Free R value: a novel statistical quantity for assessing the accuracy of crystal structures. *Nature* 355:472.
11. McCoy AJ*, et al.* (2007) Phaser crystallographic software. *Journal of applied crystallography* 40(Pt 4):658-674.
12. Huang DB, Ainsworth C, Solomon A, & Schiffer M (1996) Pitfalls of molecular replacement: the structure determination of an immunoglobulin light-chain dimer. *Acta crystallographica. Section D, Biological crystallography* 52(Pt 6):1058-1066.
13. Emsley P, Lohkamp B, Scott WG, & Cowtan K (2010) Features and development of Coot. *Acta Crystallogr D Biol Crystallogr* 66(Pt 4):486-501.
14. Murshudov GN, Vagin AA, & Dodson EJ (1997) Refinement of macromolecular structures by the maximum-likelihood method. *Acta crystallographica. Section D, Biological crystallography* 53(Pt 3):240-255.
15. Chen VB*, et al.* (2010) MolProbity: all-atom structure validation for macromolecular crystallography. *Acta Crystallogr D Biol Crystallogr* 66(Pt 1):12-21.
16. Yuwen T, Kay LE, & Bouvignies G (2018) Dramatic Decrease in CEST Measurement Times Using Multi-Site Excitation. *Chemphyschem* 19(14):1707-1710.
17. Kloiber K, Spitzer R, Grutsch S, Kreutz C, & Tollinger M (2011) Longitudinal exchange: an alternative strategy towards quantification of dynamics parameters in ZZ exchange spectroscopy. *J Biomol NMR* 51(1-2):123-129.
18. Bai Y, Milne JS, Mayne L, & Englander SW (1993) Primary structure effects on peptide group hydrogen exchange. *Proteins* 17(1):75-86.
19. Farrow NA, Zhang O, Forman-Kay JD, & Kay LE (1994) A heteronuclear correlation experiment for simultaneous determination of 15N longitudinal decay and chemical exchange rates of systems in slow equilibrium. *J Biomol NMR* 4(5):727-734.
20. Yuwen T, Kay LE, & Bouvignies G (2018) Dramatic Decrease in CEST Measurement Times Using Multi-Site Excitation. *Chemphyschem*.

21. McConnell HM (1958) Reaction Rates by Nuclear Magnetic Resonance. *The Journal of Chemical Physics* 28(3):430-431.
22. Wall J*, et al.* (1999) Thermodynamic instability of human λ 6 light chains: correlation with fibrillogenicity. *Biochemistry* 38(42):14101-14108.
23. Pokkuluri PR, Solomon A, Weiss DT, Stevens FJ, & Schiffer M (1999) Tertiary structure of human lambda 6 light chains. *Amyloid : the international journal of experimental and clinical investigation : the official journal of the International Society of Amyloidosis* 6(3):165-171.
24. Brumshtein B*, et al.* (2015) Inhibition by small-molecule ligands of formation of amyloid fibrils of an immunoglobulin light chain variable domain. *Elife* 4:e10935.